7 SCIENTIFIC HIGHLIGHT OF THE MONTH: "Recent Developments in KKR Theory"

Recent Developments in KKR Theory

H. Ebert, S. Bornemann, J. Braun, D. Ködderitzsch, S. Lowitzer, S. Mankovskyy, J. Minár, M. Offenberger, S. Polesya, and V. Popescu[1]

Universität München, Dept. Chemistry, Physical Chemistry
Butenandtstr. 5-13, D-81377 München, Germany

Abstract

In contrast to its original version that deals with the band structure of periodically ordered solids more or less like any other all-electron band structure method, the modern version of the KKR (Korringa-Kohn-Rostoker) method represents the electronic structure of a system directly and efficiently in terms of its single-particle Green's function (GF). This appealing feature and the wide applicability connected with it, is achieved by the use of multiple scattering theory (MST) for the electronic structure calculations. The basic ideas behind the resulting KKR-GF-method are outlined and the various techniques to deal with the underlying multiple scattering problem are reviewed. The second part of the contribution presents various applications of the KKR-GF-method meant to demonstrate its great flexibility and wide applicability. These should also reflect the many developments of the KKR-GF-method or methods based on it, respectively, that were made during the last years by many work groups.

7.1 Introduction

The KKR method for electronic structure calculations goes back to the work of Korringa [1], and Kohn and Rostoker [2], who introduced the original version of the scheme for periodically ordered solids. In contrast to other all-electron band structure methods based on the variational principle the KKR starts from the Schrödinger equation formulated as an integral equation; i.e. the Lippmann-Schwinger equation for Bloch states involving the free-electron Green's function $G^0(\vec{r}, \vec{r}\,', E)$. This was expected to lead to higher accuracy compared to other methods. The ansatz for the Bloch wave function used within the KKR-method implies a minimal basis set provided by energy and angular momentum dependent partial waves, with a corresponding low dimension resulting for the eigenvalue problem. Since its introduction the KKR method has been continuously further developed[2] with its domain of application enormously widened. This

[1] present address: National Renewable Energy Laboratory, Golden, Colorado, USA

[2] In fact, the title of the contribution has been borrowed from a status report given on occasion of a conference on band structure techniques in 1972 [3].

is primarily based on the fact that the KKR scheme can be interpreted in terms of multiple scattering theory (MST). This implies that the KKR method is not restricted to periodic solids but can also be applied to finite systems as well, leading to Slater's Xα-multiple scattering method for molecules [4]. Although a minimal basis set is used, the KKR-method is numerically quite demanding in practice because one has to evaluate the free-electron Green's function $G^0(\vec{r}, \vec{r}\,', E)$ in terms of so-called structure constants. Nevertheless, a rather efficient version of the KKR-method could be implemented by Moruzzi, Janak, and Williams [5] who summarised their results for pure elements in a well-known book [6]. However, as the KKR-method uses energy-dependent basis functions its original version based on the variational principle does not lead to a simple algebraic eigenvalue problem, but the energy eigenvalues have to be searched by scanning the energy with zeros of the secular determinant indicating the eigenvalues. This great drawback was removed by Andersen introducing the linear approximation for the basis functions [7]. As a consequence the original KKR-method is rarely used anymore nowadays as it was replaced by the LMTO (linear muffin-tin orbital) method as its linearised version.

This sounds like the fate of a prehistoric creature. This is by no means the case, as there is another branch of developments on the KKR-method.[3] It seems that it was Beeby who first realized that the KKR-formalism or, equivalently, multiple scattering theory can be used to get access to the Green's function (GF) of the system under consideration [8], leading finally to the KKR-GF-method. Representing the electronic structure in terms of the Green's function gives a large number of advantages as compared to the use of eigenvalues and eigenfunctions. Beeby exploited these when considering properties of substitutional impurities in solids that break the Bloch symmetry [8]. Another example is the treatment of disorder in alloys for which Korringa [9] and Beeby [10] suggested the average t-matrix approximation (ATA). In the following the basic ideas of the KKR-GF-method are sketched. In particular, the many developments of the scheme that have been made during the last two or three decades are reviewed. The various applications presented are meant to demonstrate the great flexibility of the KKR-GF-method as it is used and further developed by many active groups throughout the world.[4] The close connection between the original version of the KKR and the LMTO-method was already mentioned. Accordingly, the properties and features of the KKR-GF described will in general also apply to the TB-LMTO-GF [11] and the EMTO [12] methods as these also supply the electronic Green's function. In fact, several developments of the KKR-GF-method go back to corresponding work on these methods [11, 13].

7.2 Basic idea of the KKR-GF method

The KKR method is based on a decomposition of a system (molecule, atomic cluster, solid etc.) into atomic regions. Originally, this was done using the muffin-tin-construction (see Fig. 1). To calculate the electronic structure of the total system, as a first step an atomic region is treated as an isolated system embedded in a free-electron environment. Solving this single-site problem in a non-relativistic way implies to calculate the angular momentum l- and energy-dependent solutions $R_l(r, E)$ of the radial Schrödinger equation for a given potential. In a next step the

[3] otherwise this contribution would end here

[4] See for example the website www.kkr-gf.org that was installed very recently.

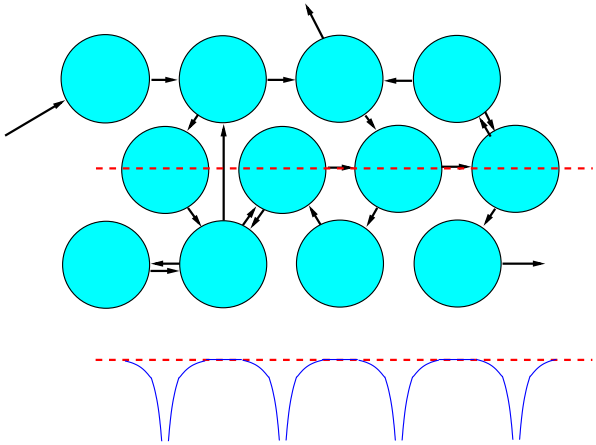

Figure 1: Central idea of multiple scattering theory: decomposition of electronic motion into scattering at atomic sites and free-electron like propagation in between. The bottom of the figure gives a sketch for the potential along the dashed line.

solutions inside the atomic regions are matched coherently with each other assuming a free-electron like behaviour in the inter-atomic or interstitial region [14]. Obviously, matching can be achieved only for certain energies corresponding to the energy eigenvalues of the system. These are found by solving a secular equation expressed in terms of the properties of the radial wave functions $R_l(r, E)$ at the boundary of the atomic regions and a structural matrix $G^{0\,nn'}_{LL'}(E)$ connecting atomic sites n and n', with $L = (l, m)$ representing the orbital angular momentum and magnetic quantum numbers. Obviously, the eigenvectors to the secular equation together with the radial functions $R_l(r, E)$ determine the eigenfunction of the total system. The l-dependency of the basis functions $R_l(r, E)\, Y_L(\hat{r})$, with $Y_L(\hat{r})$ a spherical harmonic, allows for a chemically intuitive interpretation of the results and leads to a minimal basis set. For example, for transition metals it is in general sufficient to use basis functions up to $l_{max} = 2$ rendering the KKR-method a minimal basis set method. In addition, using numerical energy-dependent basis functions obviously ensures corresponding accuracy for the eigenvalues and eigenfunctions. The energy-dependency of the basis functions, however, leads to the great disadvantage that the resulting secular equation does not correspond to an algebraic eigenvalue problem but the eigenvalues have to be found by scanning the energy through an appropriate regime. For this reason the original KKR-method as an eigenvalue scheme is hardly used any more nowadays for self-consistent electronic structure calculations.

Instead of interpreting the scheme sketched above as a mere matching technique one can interpret it in terms of multiple scattering theory. The potential connected with an atomic region gives rise to scattering of an incoming electronic wave into an outgoing one. With the partial wave functions $R_l(r, E)$ available this can be represented by a phase shift $\delta_l(E)$ or in a more general way by a corresponding single-site scattering t-matrix $t^n_{LL'}(E)$. The free-electron like propagation between scattering centres is described by the free-electron Green's function $G^0(\vec{r}, \vec{r}\,', E)$. Within the adopted angular momentum representation this is expressed in terms of the structural Green's function matrix $G^{0\,nn'}_{LL'}(E)$ already mentioned. The matching condition referred to above, now corresponds to the requirement that the wave function coming in at an atomic site has to be identical to the superposition of the waves outgoing from all other sites. This

point of view not only gives access to the energy eigenvalues and eigenfunctions of the system (see above) but also in a rather direct way to its single electron Green's function $G(\vec{r}, \vec{r}', E)$. The main features of the resulting KKR-Green's function (KKR-GF) method, that keeps all attractive features of the original KKR-method but avoids the tedious eigenvalue search, are reviewed in the following.

7.3 The single-site problem

Having chosen the decomposition of space (muffin-tin-, ASA- or Wigner-Seitz-construction), the underlying Hamiltonian (non-, scalar- or fully relativistic) including a potential term (e.g. a DFT-LSDA potential), the first step of any KKR-GF calculation is to seek the exact numerical solution of the resulting single-site problem, i.e. the energy dependent scattering solution of the given single electron Hamiltonian. For a spherical potential the corresponding solutions have pure angular momentum character L. On the other hand, for aspherical (also termed "full") potentials centred at atomic sites n and represented by an angular momentum expansion [15–19]:

$$V^n(\vec{r}) = \sum_{L}^{l_{max}^{(V)}} V_L^n(r)\, Y_L(\hat{r}) \tag{1}$$

the potential terms $V_L^n(r)$ with $L \neq (0,0)$ lead to a coupling of angular momentum channels and non- or scalar-relativistic solutions of the form

$$R_L^n(\vec{r}, E) = \sum_{L'}^{l_{max}} R_{L'L}^n(\vec{r}, E)\, Y_L(\hat{r}) \; . \tag{2}$$

The partial wave functions $R_{LL'}^n(\vec{r}, E)$ have to be determined by solving a set of coupled radial differential equations. This may be done directly or by making use of a Born series expansion [18, 20]. The latter approach is very efficient as it starts from a solution to the spherical part of the potential and accounts for the non-spherical terms in an iterative way. For spin-polarised systems and a collinear spin configuration assumed, calculations for spin up and down are done subsequently for a spin-dependent scalar potential. For non-collinear spin configurations it is advantageous to solve the single-site problem using a local frame of reference with its z-direction along the magnetic moment of the considered atomic region [21]. If the variation of the magnetisation direction within the atomic region can be ignored, the spin-dependent part of the potential is diagonal with respect to the spin and one again has a standard spin-dependent problem to solve. In case that the variation of the magnetisation is non-negligible the Born series technique can be applied again starting from the solution to the collinear part of the potential [22]. Obviously, the resulting solutions have no unique spin character any more.

Having solved for the wave functions up to a angular momentum cut-off, l_{max}, the single-site t-matrix $t_{LL'}^n(E)$ is obtained from the wave functions $R_L^n(\vec{r}, E)$ at the boundary of the atomic region. To set up the Green's function $G(\vec{r}, \vec{r}', E)$, the wave functions $R_L^n(\vec{r}, E)$ are normalised using the t-matrix giving the normalised wave functions $Z_L^n(\vec{r}, E)$, that are regular at the origin [23]. In addition, an irregular wave function $J_L^n(\vec{r}, E)$ has to be calculated in an analogous way (see below), that fulfils certain boundary conditions at the surface of the atomic regime [23]. For fully relativistic calculations on the basis of the four-component Dirac formalism [24], the

situation is completely analogous with the spherical harmonics $Y_L(\hat{r})$ replaced by spin-angular functions $\chi_\Lambda(\hat{r})$ ($\Lambda = (\kappa, \mu)$ with κ and μ the relativistic spin-orbit and magnetic quantum numbers) and the radial wave functions $R^n_L(\vec{r}, E)$ by the large and small components $g^n_\kappa(r, E)$ and $f^n_\kappa(r, E)$, respectively [25]. Calculations for spin-polarised systems, however, become more complicated now as the spin-dependent part of the potential breaks the full rotational symmetry and leads to a coupling of partial waves as in Eq. (2) even if one restricts to spherical potential functions ($l^{(V)}_{max} = 0$ in Eq. (1)) [26, 27]. In the most general situation the potential couples not only to the spin but also to the orbital degree of freedom of the electron. This holds for calculations within CDFT (current density functional theory) [28], if the Breit interaction is included within fully relativistic calculations [29] or if correlation effects are treated by a scheme going beyond standard LDA (see below). This situation can be dealt with in analogy to the spin-dependent case leading to more terms to be considered for the set of coupled radial equations. As long as the orbital-dependent terms do not change the symmetry, however, the number of coupled wave functions (corresponding to the sum over L' in Eq. (2)) does not change.

For situations in which the LDA or LSDA, respectively, seem to be inadequate, one may set up the potential defining the single-site problem in a more sophisticated way. In the case of the non-relativistic spherical implementation of the so-called local SIC (self interaction correction) [30,31] this does not cause any technical problems as the potential becomes only l-dependent with no coupling among the partial waves induced. For the OP (orbital polarisation) [32], the LDA+U [33], as well as the DMFT (dynamical mean field theory) [34], on the other hand, the effective potential depends on the m-character of the wave function in addition. This implies that the corresponding single-site problem has to be dealt with on a full-potential level. In particular it turns out that the additional potential terms occurring within the LDA+U and DMFT schemes are strictly spoken non-local. For the DMFT, with the correlation effects represented by a self-energy matrix $\Sigma_{LL'}(E)$, these become complex and energy-dependent dependent in addition [34].

When solving the single-site problem, obviously the entire complexity of the underlying geometrical description and Hamiltonian (aspherical potential, non-collinear magnetism, spin-orbit coupling, Breit interaction, non-local potentials within LDA+U or DMFT etc.) is accounted for. Accordingly, the resulting regular and irregular wave functions $Z^n_L(\vec{r}, E)$ and $J^n_L(\vec{r}, E)$ as well as the corresponding single-site t-matrix $t^n_{LL'}(E)$ carry all information on the complete Hamiltonian. The resulting single-site solutions could of course be used as numerical basis functions within any all-electron method that determines energy eigenvalues and eigenfunctions on the basis of the variation principle; as e.g. the LAPW, LMTO or ASW. Apart from few exceptions, as for example in the spin-polarised relativistic case [35, 36], this is hardly done. Instead solutions to a simplified scalar-relativistic single-site problem with a spherical potential are used in general, dealing with all additional complexity of the Hamiltonian within the variational step.

7.4 Multiple scattering

With the single-site t-matrix available the next step of a KKR-GF calculation is to solve the multiple scatting problem. This task can be solved very elegantly by using the scattering path operator $\tau^{nn'}$ introduced by Györffy and Stott [37], that transfers an electronic wave incoming at site n' into a wave outgoing from site n with all possible scattering events that may take place

in between in a self-consistent way. Adopting an angular momentum representation (see above) this requirement implies for the corresponding matrix the following implicit equation of motion

$$\underline{\tau}^{nn'}(E) = \underline{t}^{n}(E)\,\delta_{nn'} + \underline{t}^{n}(E)\sum_{k\neq n}\underline{G}^{0\,nk}(E)\,\underline{\tau}^{kn'}(E)\;, \tag{3}$$

with $(\underline{\tau}^{nn'})_{LL'} = \tau^{nn'}_{LL'}$ etc. For a finite system this equation is solved straight forwardly by a matrix inversion [38]:

$$\underline{\underline{\tau}}(E) = [\underline{\underline{t}}(E)^{-1} - \underline{\underline{G}}^{0}(E)]^{-1}\;, \tag{4}$$

where $\underline{\underline{M}} = [\underline{\underline{t}}^{-1} - \underline{\underline{G}}^{0}]$ is the so-called real-space KKR-matrix, with $[\underline{\underline{\tau}}]^{nn'} = \underline{\tau}^{nn'}$, $[\underline{\underline{G}}^{0}]^{nn'} = \underline{G}^{0\,nn'}$ and $[\underline{\underline{t}}]^{nn'} = \underline{t}^{n}\delta_{nn'}$.[5] Obviously, the dimension of the various matrices is determined by the number of sites (atoms) in the system and the angular momentum cut-off l_{max}. For a non- or scalar-relativistic formulation $\underline{\underline{G}}^{0}$ can be calculated easily from analytical expressions. For the fully relativistic case $\underline{\underline{G}}^{0}$ is obtained from its non-relativistic counterpart by a simple Clebsch-Gordan transformation [39]. For a finite system the solution to the multiple scattering problem given by Eq. (4) is obviously exact. It is also useful if an extended system is approximated by a finite subsystem as it is justified for example when dealing with EXAFS spectra [39, 40]. A cluster representation of the atomic environment is also used within the locally self-consistent multiple scattering (LSMS) method [41]. As each inequivalent atom is represented by its own cluster or local interaction zone (LIZ), respectively, the method scales strictly with the system size N leading to an Order-N method.

Dealing with a three-dimensional periodic system Eq. (3) can also be solved exactly by Fourier transformation leading to [23]:

$$\underline{\tau}^{nn'}(E) = \frac{1}{\Omega_{\mathrm{BZ}}}\int\limits_{\Omega_{\mathrm{BZ}}} d^3k\,[\underline{t}(E)^{-1} - \underline{G}^{0}(\vec{k},E)]^{-1}\,e^{i\vec{k}(\vec{R}_n - \vec{R}_{n'})}\;, \tag{5}$$

with the (reciprocal space) structure constants matrix $\underline{G}^{0}(\vec{k},E)$ being the Fourier transformed of the real-space structure constants matrix $\underline{\underline{G}}^{0}(E)$. Accordingly, working on a fully relativistic level $\underline{G}^{0}(\vec{k},E)$ is again obtained from its non-relativistic counterpart by a simple Clebsch-Gordan transformation [42].

The KKR-matrix $\underline{M}(\vec{k},E) = [\underline{t}(E)^{-1} - \underline{G}^{0}(\vec{k},E)]$ in Eq. (5) is identical to the secular matrix occurring within the original KKR method. Accordingly, varying the energy E for the wave vector $\vec{k}$ fixed $\underline{M}(\vec{k},E)$ will indicate an eigenvalue $E_{\vec{k}}$ by a jump of its phase. This interrelation is the basis for Lloyd's formula [43–46] that gives the integrated density of states $N(E)$ in terms of the imaginary part of the logarithm of the determinant of $\underline{M}(\vec{k},E)$. This approach can be applied not only to ordered and disordered (see below) solids [47, 48] but also to finite systems [49]. It allows in particular to handle the single particle energy term within total energy calculations in a very elegant way [48]. Closely connected with this, Lloyd's formula gives a very sound basis when dealing with magnetic properties, like the exchange coupling constants J_{ij} (see below), on the basis of the so-called magnetic force theorem [50, 51].

The calculation of the structure constants matrix $\underline{G}^{0}(\vec{k},E)$ was for a long time the bottleneck when applying the original KKR-method. However, several schemes have been developed for an

[5] The energy argument has been dropped here and in the following where appropriate.

efficient evaluation of $\underline{G}^0(\vec{k},E)$ [5,52] allowing to calculate it on-the-fly with much less effort than needed to invert the KKR-matrix $\underline{M}(\vec{k},E)$. For systems having only two-dimensional periodicity appropriate schemes have been developed as well to solve the corresponding multiple scattering problem leading to the so-called layer KKR (LKKR) method [53, 54]. These are extensively used when dealing with LEED [55] or angle-resolved photo emission (ARPES) [56] but also for SCF-calculations for layered systems [54]. The numerical effort to deal with the Brillouin zone integral in Eq. (5) or its two-dimensional counterpart can substantially be reduced if the symmetry of the system is exploited. For this purpose a scheme was worked out to find the non-zero matrix elements and to reduce the integration regime to the irreducible part of the Brillouin zone [57]. The scheme is applicable in particular for the spin-polarised relativistic case for which unitary as well as anti-unitary magnetic point group operations have to be considered. In addition, it allows also to handle more complex Brillouin zone integrals involving products of scattering path operators occurring in the context of linear response formalism (see below).

7.5 The single electron Green's function and Dyson's equation

Having solved the multiple scattering problem the retarded single-electron Green's function $G(\vec{r},\vec{r}\,',E)$ can be written as [23, 58]:

$$\begin{aligned} G(\vec{r},\vec{r}\,',E) &= \sum_{LL'} Z_L^n(\vec{r},E)\tau_{LL'}^{nn'}(E)Z_{L'}^{n'\times}(\vec{r}\,',E) \\ &\quad -\sum_L \big[\, Z_L^n(\vec{r},E)J_L^{n\times}(\vec{r}\,',E)\Theta(r'-r) \\ &\qquad +J_L^n(\vec{r},E)Z_L^{n\times}(\vec{r}\,',E)\Theta(r-r')\,\big]\,\delta_{nn'}\;, \end{aligned} \tag{6}$$

where $\vec{r}$ ($\vec{r}\,'$) lies in the atomic cell n (n') representing cell-centred coordinates and $\times$ indicates a so-called left-hand side solution [59]. If the spin of the electron is accounted for explicitly, e.g. when dealing with non-collinear spin-configurations the Green's function $G(\vec{r},\vec{r}\,',E)$ is a 2×2-matrix function [22]. In case of fully relativistic calculations using four-component wave functions $Z_\Lambda^n(\vec{r},E)$ and $J_\Lambda^n(\vec{r},E)$, respectively, $G(\vec{r},\vec{r}\,',E)$ is a 4×4-matrix function [29].

The expression for $G(\vec{r},\vec{r}\,',E)$ given in Eq. (6) follows in a natural way if multiple scatting is represented by the scattering operator $\underline{\underline{\tau}}$ with a corresponding normalisation of the wave functions (Bristol-Oak-Ridge convention). An alternative to this is to use the so-called structural Green's function matrix $\underline{\underline{G}}$ instead that is related to $\underline{\underline{\tau}}$ by $\underline{\underline{G}} = \underline{\underline{t}}^{-1}\underline{\underline{\tau}}\,\underline{\underline{t}}^{-1} - \underline{\underline{t}}^{-1}$ together with regular and irregular wave functions $R_L^n(\vec{r},E)$ and $H_L^n(\vec{r},E)$, respectively, normalised accordingly (Jülich convention) [60].

With the Green's function $G(\vec{r},\vec{r}\,',E)$ available all properties of interest can be calculated straight forwardly. For example the particle density $n(\vec{r})$ and density of states $n(E)$ are given by:

$$n(E) = -\frac{1}{\pi}\,\Im\,\mathrm{Trace}\int_{\Omega_n} d^3r\, G(\vec{r},\vec{r},E) \tag{7}$$

$$\rho(\vec{r}) = -\frac{1}{\pi}\,\Im\,\mathrm{Trace}\int^{E_F} dE\, G(\vec{r},\vec{r},E)\;, \tag{8}$$

where the trace applies if $G(\vec{r},\vec{r}\,',E)$ is given in matrix form. It's worth to note that for $n(E)$ and $\rho(\vec{r})$, needed for example within SCF calculations, only site-diagonal scattering path operators

$\underline{\tau}^{nn}$ are required. For a more detailed representation of the electronic structure than supplied by the DOS $n(E)$, the Bloch spectral function $A_{\rm B}(\vec{k},E)$ may be used that is defined as the Fourier transformed of $G(\vec{r},\vec{r}\,',E)$ [58]:

$$A_{\rm B}(\vec{k},E) = -\frac{1}{\pi N}\,\Im\,\mathrm{Trace}\sum_{n,n'}^{N} e^{\imath\vec{k}(\vec{R}_n-\vec{R}_{n'})}\int_{\Omega} d^3r\, G\left(\vec{r}+\vec{R}_n,\vec{r}+\vec{R}_{n'},E\right)\,. \tag{9}$$

Thus, $A_{\rm B}(\vec{k},E)$ can be seen as a $\vec{k}$-resolved density of states function. For a perfectly ordered system, in particular, $A_{\rm B}(\vec{k},E)$ is just a sum of δ-functions $\delta(E-E_{\vec{k}})$ that represents the usual dispersion relation $E_{\vec{k}}$.

Obviously, the KKR-GF method supplies all information on the electronic structure that may also be supplied by any other band structure method that represents the electronic structure in terms of energy eigenvalues and eigenfunctions. However, using the Green's function from the very beginning to represent the electronic structure provides a large number of advantages.

The definition of the Green's function and all expressions given above is not restricted to real energies E but also holds for arbitrary complex energies z.[6] The fact that $G(\vec{r},\vec{r}\,',E)$ is analytical [61] allows, in particular, to perform the energy integration in Eq. (8) on a contour in the complex energy plane [62,63] with typically around 30 energy mesh points needed. This results in an efficiency comparable to linear band structure methods without making use of the linear approximation (with respect to the energy) for the basis functions [64].

One of the major benefits of working with the Green's function $G(\vec{r},\vec{r}\,',E)$ is the use of the Dyson equation:

$$G(\vec{r},\vec{r}\,',E) = G^{\rm ref}(\vec{r},\vec{r}\,',E) + \int_{\Omega_{\rm pert}} d^3r''\, G^{\rm ref}(\vec{r},\vec{r}\,'',E)\,\mathcal{H}_{\rm pert}(\vec{r}\,'')\,G(\vec{r}\,'',\vec{r}\,',E)\,. \tag{10}$$

This equation allows to get the Green's function $G(\vec{r},\vec{r}\,',E)$ of a system described by a Hamiltonian $\mathcal{H}=\mathcal{H}_{\rm ref}+\mathcal{H}_{\rm pert}$ in terms of the Greens function $G^{\rm ref}(\vec{r},\vec{r}\,',E)$ for a simpler reference system described by $\mathcal{H}_{\rm ref}$ and a perturbation $\mathcal{H}_{\rm pert}$. In fact, this equation supplies the formal background for the scheme sketched above where the free-electron system supplies the reference system, i.e. $G^{\rm ref}(\vec{r},\vec{r}\,',E)=G^0(\vec{r},\vec{r}\,',E)$, and the perturbation $\mathcal{H}_{\rm pert}$ is given by the potential $V(\vec{r})$ of the system to be considered.

The Dyson equation allows for many interesting situations to deal with the multiple scattering problem in a very efficient way. Replacing the single-site scattering t-matrix of the real system by t-matrices $\underline{t}^{\rm TB}$ that are derived from a repulsive potential one gets by solving the corresponding multiple scattering problem the Green's function $G^{\rm TB}(\vec{r},\vec{r}\,',E)$ for this artificial new reference system. In contrast to the free-electron Green's function $G^0(\vec{r},\vec{r}\,',E)$, this new auxiliary Green's function $G^{\rm TB}(\vec{r},\vec{r}\,',E)$ decays very rapid in space, i.e. with increasing distance $|\vec{r}-\vec{r}\,'|$. As a consequence the corresponding scattering path operator $\underline{\tau}^{{\rm TB}\,nn'}$ is essentially zero if the distance of sites n and n' is greater than the next-nearest neighbour distance. Solving now the multiple scattering problem for the real system using the Green's function of the new reference system

[6] The symbol E will still be used in the following for the energy, without implying a restriction to the real axis.

one gets for its scattering path operator $\underline{\underline{\tau}}$ the following set of equations [60]:

$$\underline{\underline{G}}^{\mathrm{TB}} = \underline{\underline{G}}^{0}\,[\underline{\underline{1}} - \underline{\underline{t}}^{\mathrm{TB}}\,\underline{\underline{G}}^{0}]^{-1} \tag{11}$$

$$\underline{\underline{\tau}}_{\Delta} = [\Delta\underline{\underline{t}}^{-1} - \underline{\underline{G}}^{\mathrm{TB}}]^{-1} \tag{12}$$

$$\Delta\underline{\underline{t}} = \underline{\underline{t}} - \underline{\underline{t}}^{\mathrm{TB}} \tag{13}$$

$$\underline{\underline{G}} = (\Delta\underline{\underline{t}}^{-1})\,\underline{\underline{\tau}}_{\Delta}\,(\Delta\underline{\underline{t}}^{-1}) - (\Delta\underline{\underline{t}}^{-1})\,. \tag{14}$$

Because of the sparseness of the matrix $\underline{\underline{G}}^{\mathrm{TB}}$ one has now a sparse matrix problem to deal with as for the tight binding (TB) formalism. The main idea behind the resulting TB-KKR-GF [60, 65] goes back to a similar scheme used within the TB-LMTO [66]. Analogous to this case the TB-KKR-GF method becomes an order(N)-method with its numerical effort scaling linearly with the system size if the structure of the system can be exploited [60]. Using an efficient scheme to deal with the auxiliary TB-reference system, this allows to deal with systems containing thousands of atoms [67].

So far the TB-KKR-GF has been primarily applied to two-dimensional periodic layered systems for which a hybrid representation of the scattering path operator $\underline{\tau}^{II'}(\vec{k}_{\parallel}, E)$ is used, with I and I' layer indices and $\vec{k}_{\parallel}$ a vector of the corresponding two-dimensional reciprocal space. For a given $\vec{k}_{\parallel}$ the multiple scattering problem with respect to the layer index has then a TB-structure, that can be solved with established techniques [11, 65].

As an example Fig. 2 shows results of TB-KKR-GF calculations for a Co mono layer on top of a Pt(111) substrate. For the first calculation the substrate was approximated by a slab of

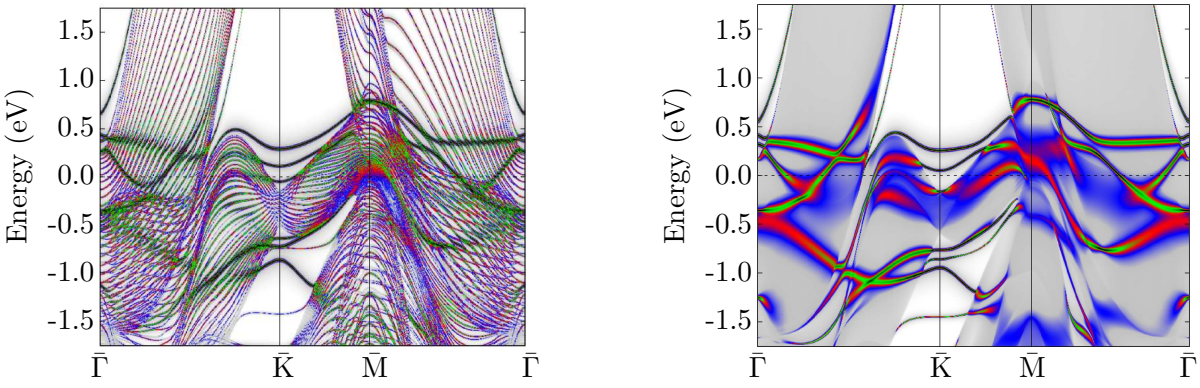

Figure 2: Co-projected Bloch spectral function $A_{\mathrm{B}}(\vec{k}_{\parallel}, E)$ for a Co mono-layer on top of a Pt (111) substrate. Left: a slab geometry with 38 atomic layers was used. Right: the Pt(111) substrate was represented by a semi-infinite solid.

38 (111)-oriented Pt-layers. The Bloch spectral function $A_{\mathrm{B}}(\vec{k}, E)$ projected onto the Co-layer shown in Fig. 2 (left) can now be seen as a $\vec{k}_{\parallel}$-resolved partial DOS of Co. Obviously, it shows many discrete bands that are caused by the spatial confinement imposed by the slab geometry. Dealing with a Co-mono layer on top of a semi-infinite Pt(111) substrate instead, the artificial confinement is removed and the spurious features of the local electronic structure are gone.

7.6 Embedding of atoms clusters in a perfect host system

For the examples considered above the reference system for the Dyson equation is just a suitable auxiliary system. Another important application of the Dyson equation is the embedding of a perturbing subsystem into a host reference system. The most simple case is the substitutional embedding of an impurity atom into an otherwise perfect three-dimensional periodic host, with a perturbation of its neighbouring atoms. Because the impurity breaks the Bloch symmetry of the system standard band structure schemes can handle the problem only by using the super cell approach. To keep the interaction of neighbouring impurity cells negligible, large enough super cells have to be used.

This problem can be completely avoided by making use of the Dyson equation. Dealing with a metallic host the perturbation caused by a substitutional impurity is typically restricted to few neighbouring atomic shells due to screening. The integration regime $\Omega_{\rm pert}$ in Eq. (10) can be restricted accordingly. Representing the Green's functions by means of multiple scattering theory Eq. (6) the Dyson equation is transformed to an equivalent algebraic equation for the scattering operator that can be solved easily:

$$\underline{\underline{\tau}}^{\rm imp} = [(\underline{\underline{t}}^{\rm imp})^{-1} - (\underline{\underline{t}}^{\rm host})^{-1} - (\underline{\underline{\tau}}^{\rm host})^{-1}]^{-1} \; , \tag{15}$$

where the site index of the matrices is restricted to the atomic sites within the regime $\Omega_{\rm pert}$. In Eq. (15) $\underline{\underline{\tau}}^{\rm host}$ is the scattering path operator matrix for the corresponding cluster of unperturbed host atoms with single site t-matrices $\underline{\underline{t}}^{\rm host}$. $\underline{\underline{\tau}}^{\rm imp}$ is the scattering path operator matrix representing the embedded atom cluster with the substitutional impurity atom at the centre and the single site matrices collected in $\underline{\underline{t}}^{\rm imp}$. As mentioned, the size of the cluster can be restricted typically to few neighbouring atomic shells around the impurity atom. For specific problems much larger clusters may be necessary. An example for this is the investigation of satellites in Cu-NMR that can be ascribed to Cu-atoms in the vicinity of a magnetic 3d-impurity atom. In experiment signals from Cu-atoms up to the 6^{th} neighbouring shell could be identified and confirmed by KKR-GF-based calculations [68]. Another example is an investigation of the so-called giant magnetic moments caused by the spin-polarisation of Pd in the vicinity of an embedded magnetic 3d-impurity atom. In this case even for clusters with 8 atomic shells around the impurity, containing 683 atoms all together, an appreciable polarisation of the Pd atoms on the outermost cluster shell was found [69].

In Fig. 3 the first results of a more exotic application of the embedding scheme are presented. The left part of the figure shows the electronic charge distribution around a vacancy in Al. From this the corresponding potential seen by a positron was constructed [70] and a KKR-GF calculation for the positron was performed subsequently. The right panel of Fig. 3 shows the corresponding DOS for the positron on the vacancy and the neighbouring Al sites. As one can see a bound state for the positron emerges that is localised on the vacancy site. From the DOS for the neighbouring Al sites it is clear that the positron state is not completely restricted to the vacancy regime but spills out over the neighbouring sites. In fact, only about 63 % of the positron charge is localised at the vacancy site. The corresponding charge distribution for a single positron trapped on the vacancy site shown in the middle panel of Fig. 3 demonstrates this as well. It should be noted that the lifetime of the positron that can be measured in experiment

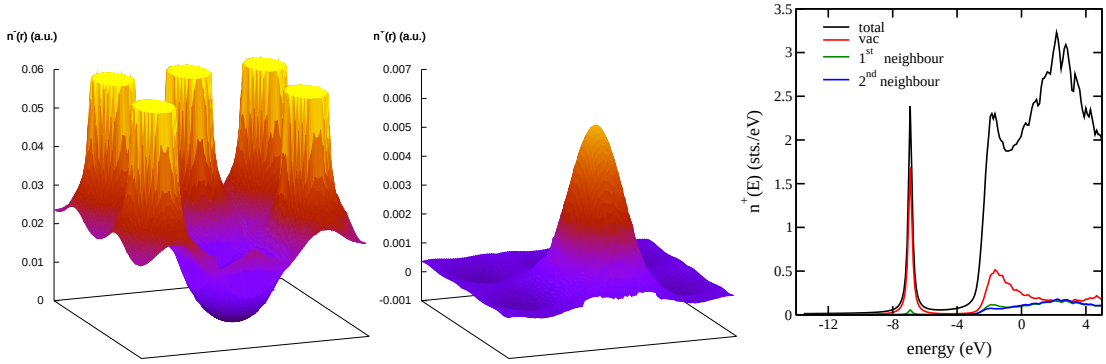

Figure 3: Left: electronic charge distribution $n^-(\vec{r})$ around a vacancy in fcc-Al showing the charge depletion at the vacancy site. Middle: charge distribution $n^+(\vec{r})$ for a single positron trapped in the vacancy regime. Right: DOS $n^+(E)$ for the positron on the vacancy and Al sites of the neighbouring two atom shells, respectively. The δ-like peak for the bound positron state is smeared out to a Lorentzian line due to the use of complex energies with a corresponding imaginary part.

is determined by the overlap of the positronic and electronic charge distributions [70]. As it is obvious from the results shown in Fig. 3 the lifetime of the positron will be modified if an additional impurity atom becomes nearest neighbour to the vacancy. In fact, positron life time measurements are a well established experimental tool to investigate impurity-vacancy dimers that play a very important role for metallurgical properties [70].

The embedding scheme described above is of course not restricted to three-dimensional bulk systems as a host but can be applied straight forwardly to clusters deposited on a substrate. This was demonstrated by many investigations on the magnetic properties of transition metal clusters deposited on various substrates [71–74]. As a corresponding example Fig. 4 shows a pyramid-shaped cluster of Fe- and Pt-atoms with a fcc-like structure deposited on a Cu (001)-substrate. The table next to the figure gives the spin and orbital magnetic moments resulting

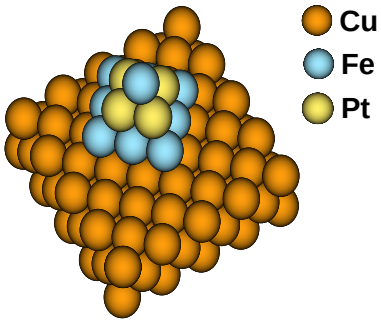

	free		supported	
	μ_{spin}	μ_{orb}	μ_{spin}	μ_{orb}
Fe top	3.016	0.206	3.004	0.195
Pt middle	0.356	0.083	0.296	0.067
Fe base	2.622	-0.019	2.322	0.003

Figure 4: Pyramid-shaped FePt-cluster with a fcc-like structure deposited on a Cu (001)-substrate. The table gives the spin and orbital magnetic moments for the deposited cluster as well as for a free cluster with the same structure.

from a fully relativistic KKR-GF calculation. The table gives in addition results of corresponding calculations for a free FePt-cluster that has the same structure as the deposited one and that has been treated by the real space version of the KKR-GF method for finite systems. As one notes the resulting spin moments for the Fe atoms are quite high and similar to that for bulk

FePt with CuAu structure. For the Fe-atom at the top of the pyramid the moments in both cluster systems are more or less the same implying that the substrate has very weak influence in the case of the deposited FePt cluster. For the Fe-atom in the middle of the basal plane of the clusters there is an appreciable difference however. As one would expect on the basis of the Stoner-criterium for spontaneous spin magnetism, the spin moment is smaller for the deposited cluster due to bond formation with the substrate and a corresponding increase of the d-band width for the Fe-atoms in the basal plane.

There are many more applications of the KKR-GF embedding technique to surface nano structures containing up to several hundreds of atoms. In particular the influence of adatoms and embedded impurity atoms on the surface electronic structure was studied in detail this way [75]. Another interesting example is the investigation of quantum corrals [76] and the occurrence of so-called mirages induced by enclosed magnetic impurity atoms [77]. Several investigations were devoted to the exchange coupling within a magnetic nano structure (see below) or the coupling of magnetic adatom moments via the substrate [78]. For finite anti-ferromagnetic nano wires deposited on a ferromagnet, the so-called even-odd effect was studied be means of non-collinear calculations showing the central importance of the number of atoms in the wire for its magnetic ground state [79]. The KKR-GF embedding scheme is applicable without modification to any other two-dimensional system. An example for this are half-infinite electrodes separated by vacuum and connected by a single wire [80,81]. In the case of magnetic wires non-collinear spin structures as well as their transport properties have been investigated even in a fully relativistic way [82].

For most KKR-GF-based embedded cluster calculations it was assumed so far that the cluster atoms occupy substitutionally perfect lattice sites of the host systems; this implies that possible lattice relaxations have been ignored. However, this is not a necessary restriction as various schemes have been worked out to account for lattice relaxations within KKR-GF calculations for embedded systems. For relatively small relaxations in the order of few percent the Green's function of the host reference system can be re-expanded around the shifted atomic positions by a so-called U-transformation [83,84]. This has been applied with great success for bulk systems [84] as well as surface systems [85]. In case of more pronounced shifts of the atomic positions or when dealing with interstitial impurities an auxiliary sub lattice can be introduced [86–88]. In addition, a scheme has been developed that allows to embed clusters with a structure completely unrelated to that of the host system as it occurs for example when dealing with segregation in a bulk material [89, 90].

7.7 Treatment of chemical disorder

Dealing with disordered substitutional alloys the chemical disorder destroys obviously the Bloch symmetry even if a perfect underlying lattice is assumed. Using a standard band structure method this situation can again be handled only by making use of the super cell technique. This implies that one is restricted to concentrations that can be represented by stoichiometric compounds and that one has to use large super cells if the concentration of one of the components in the alloy is low. In addition, one has to average over several atomic configurations in the super cell to get the configurational average corresponding to the disordered state.

Attempts to construct a configurationally averaged wave function for a disordered solid does not seem to be very sensible [14]. Seeking for the configurational average of the electronic Green's function, on the other hand, makes sense and various schemes have been suggested for this purpose in particular on the basis of multiple scattering theory [14]. Obviously construction of a configurational average is most simple if any correlation concerning the occupation of neighbouring sites is ignored i.e. short-range order is excluded and a random distribution of the components is assumed with the alloy composition being the only restriction. On the basis of this single-site approximation Korringa [9] and Beeby [10] suggested to represent a disordered alloy by a single-site t-matrix $\underline{t}^{\mathrm{ATA}}$ that is obtained by the concentration-weighted average over the components; e.g. $\underline{t}^{\mathrm{ATA}} = x_{\mathrm{A}}\underline{t}^{\mathrm{A}} + x_{\mathrm{B}}\underline{t}^{\mathrm{B}}$ for a binary disordered alloy $A_{x_{\mathrm{A}}}B_{x_{\mathrm{B}}}$. This average t-matrix approximation (ATA), however, leads to a Green's function that does not guarantee a positive definite DOS for real energies. This problem could be removed in a mathematically sound way by the Coherent Potential Approximation (CPA) of Soven [91] that introduces an auxiliary CPA medium by demanding that embedding one of the components into the CPA medium should reproduce in the concentration average the properties of the CPA medium. This central idea of the CPA is represented by Fig. 5. Expressing it in terms of the KKR-GF

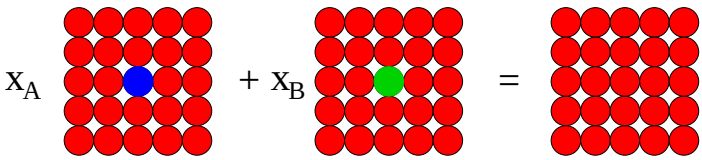

Figure 5: Basic idea of the Coherent Potential Approximation (CPA): the embedding of one of the components of an alloy $A_{x_A}B_{x_B}$ into the CPA-medium should not change its properties if the concentration-weighted average is taken.

formalism this means that the average should cause no additional scattering compared to the CPA-medium [92]:

$$x_{\mathrm{A}}\underline{\tau}^{\mathrm{A}\,nn} + x_{\mathrm{B}}\underline{\tau}^{\mathrm{B}\,nn} = \underline{\tau}^{\mathrm{CPA}\,nn} \; . \tag{16}$$

In line with the single site approximation the component projected scattering path operator matrices $\underline{\underline{\tau}}^{\alpha}$ ($\alpha = A, B$) are given by Eq. (15) with the CPA-medium as a host and the cluster size reduced to the single central atom. Eq. (16) imposes implicitly a condition to be met by the single-site t-matrix $\underline{t}^{\mathrm{CPA}}$ of the CPA-medium. In addition, $\underline{t}^{\mathrm{CPA}}$ has to lead to the CPA scattering path operator $\underline{\tau}^{\mathrm{CPA}\,nn}$, e.g. via Eq. (5). Due to this implicit definition of $\underline{t}^{\mathrm{CPA}}$ it has to be calculated by solving these so-called CPA equations iteratively starting from a reasonable guess as e.g. $\underline{t}^{\mathrm{CPA}}_{\mathrm{start}} = \underline{t}^{\mathrm{ATA}}$ [93]. The resulting description of the configurational average via $\underline{t}^{\mathrm{CPA}}$ and $\underline{\tau}^{\mathrm{CPA}\,nn}$ is the best solution that can be achieved on the basis of the single-site approximation. It can be shown, in particular, that the CPA is exact up to fourth order in the scattering t-matrices with respect to the CPA medium [91].

Within the combined KKR-GF-CPA scheme the Green's function for the alloy is given by the concentration weighted average according to Eq. (16) with [14]:

$$G(\vec{r}, \vec{r}', E) = \sum_{\alpha} x_{\alpha}\, G^{\alpha}(\vec{r}, \vec{r}', E) \; , \tag{17}$$

with the component projected Green's function G^{α} given by Eq. (16) using the component-projected $\underline{\tau}^{\alpha\,nn'}$ and specific wave functions Z^{α} and J^{α}. The expression makes clear that the CPA

provides an averaged but component specific information on the electronic structure as it may be probed by element-specific experimental techniques like NMR, Mößbauer spectroscopy [94] or XAS (x-ray absorption spectroscopy) [95].

Since its first successful numerical implementation [96] the KKR-GF-CPA scheme was applied with great success to many different alloy systems. In particular using the Bloch spectral function $A_{\mathrm{B}}(\vec{k}, E)$ for the discussion of the electronic structure of disordered systems [58] turned out to be very useful. As an example the top row of Fig. 6 shows results for the Bloch spectral function $A_{\mathrm{B}}(\vec{k}, E)$ of ferromagnetic fcc-$Fe_{0.2}Ni_{0.8}$ as a function of the energy and wave vector $\vec{k} \parallel [100]$ [97]. The uppermost plot gives the total Bloch spectral function while the plots below give its minority

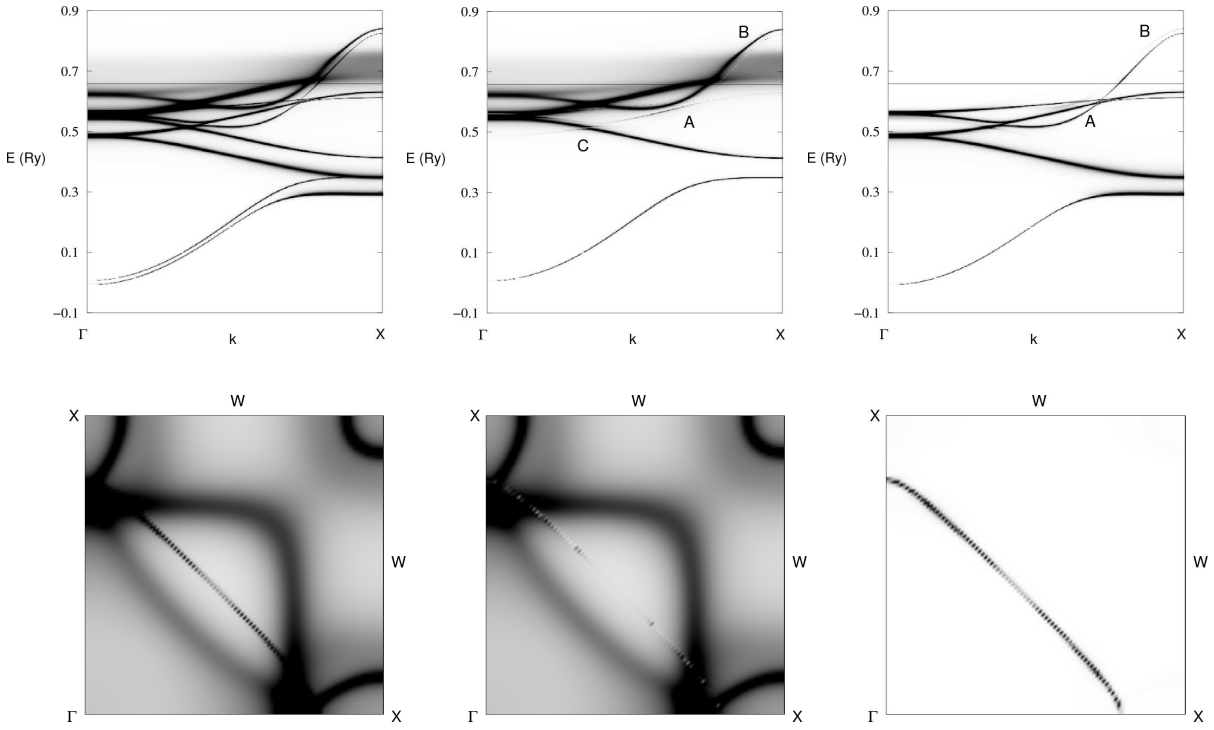

Figure 6: Top row: Gray-scale representation of the Bloch spectral function $A_{\mathrm{B}}(\vec{k}, E)$ (in atomic units) for fcc-$Fe_{0.2}Ni_{0.8}$ with $\vec{k} \parallel [100]$ and the magnetisation $\vec{M} \parallel [001]$. The white background corresponds to $A_{\mathrm{B}}(\vec{k}, E) = 0$, while the black regions represent $A_{\mathrm{B}}(\vec{k}, E) \geq 50$ a.u.; i.e. the cusps of $A_{\mathrm{B}}(\vec{k}, E)$ have been cut for a more resolved representation. The column in the middle and at the end of a row give $A_{\mathrm{B}}(\vec{k}, E)$ decomposed into their minority and majority spin part, respectively. Bottom row: $A_{\mathrm{B}}(\vec{k}, E)$, but for the energy fixed to the Fermi energy $\mathrm{E_F}$ and $\vec{k}$ lying in the (010)-plane; i.e. the horizontal axis gives the component of $\vec{k}$ perpendicular to $\vec{M}$, while the vertical axis gives that parallel to $\vec{M}$ [97].

and majority spin contribution. As one notes for the selected concentration the spectral function resembles very much the dispersion relation $E_{\vec{k}}$ of pure Ni. However, due to the disorder in the alloy the curves are smeared out implying that the wave vector $\vec{k}$ is not a good quantum number any more. In addition, one notes that the impact of disorder is much more important for the minority than for the majority spin channel. This is because the resonance of the d-states of Fe and Ni is very close to each other for the majority band while – due to the different local exchange splitting – they are shifted against each other for the minority spin channel. The same

behaviour can be seen for the plots in the bottom row of Fig. 6 that represent the Fermi surface of the alloy. The width and variation of the Bloch spectral function at the Fermi level can be used to deduce a $\vec{k}$-dependent life time $\tau_{\vec{k}}$ of the electrons and a corresponding group velocity $v_{\vec{k}}$. This has been exploited by Butler and Stocks to calculate the residual resistivity of Ag_xPd_{1-x} on the basis of the Boltzmann formalism (see below) [98].

In the middle column of Fig. 6 one notices very weak features that correspond to the majority spin spectral function. This mixing of the spin channels is caused by spin-orbit-coupling that has been accounted for by performing spin-polarised fully relativistic calculations. For the transport properties of ferromagnetic alloys this spin-mixing has important consequences as is gives among other rise to the galvano-magnetic properties; i.e. the anomalous magneto-resistance (AMR) and the spontaneous Hall-effect (SHE) [99, 100].

As mentioned before, the CPA is a single-site theory and for that reason does not give direct access to features in the electronic properties caused by short-range order (SRO). Nevertheless, as was demonstrated by Györffy and Stocks [101], SRO phenomena may be investigated in terms of concentration waves. Another route is to investigate the electronic structure of clusters with specific configurations embedded into the CPA-medium [102]. This embedded cluster method (ECM) has been used for example to study the variation of the nuclear spin lattice relaxation time of Cu and Pt in Cu_xPt_{1-x} [103] and of the hyperfine fields of Fe and Ni in fcc-Fe_xNi_{1-x} alloys [104] with their local environment. In all cases it turned out that the average over all investigated configurations agrees very well with the CPA-result.

It should be stressed that the CPA is not restricted to deal with chemical disorder in three-dimensional alloy systems but can be used for inhomogeneous systems as well. Important examples for the latter are the inter diffusion at interfaces [105–107] and surface segregation [108] for which one has to deal with a layer dependent concentration profile. Also in case of finite systems as free and deposited alloy clusters [109] the CPA has been applied successfully. Furthermore, exploiting the alloy analogy the CPA scheme was transferred to deal with the thermal fluctuations of magnetic moments in ferromagnets leading to the disordered local moment (DLM) scheme [110, 111]. Within a non-relativistic approach the single-site averaging leads for the paramagnetic state of a pure ferromagnet effectively to a binary alloy that has components with their moments oriented up and down, respectively, having each a concentration $x = 1/2$. An extension of the DLM to layered systems allowed to determine the magnetic ordering temperature for 3 and 7 layers of Fe on Cu(100) as a function of the Cu coverage in very satisfying agreement with experiment [112]. Recently, corresponding work was done for rare earth systems revealing the magnetic ordering tendencies as a function of the volume and the c/a-ratio [113]. In this case correlation effects were accounted for by making use of the local SIC [30]. Combining local SIC and CPA causes obviously no conceptual or technical problems within the KKR-GF formalism because both schemes make use of the single-site approximation. The same holds for the combination of the CPA used to deal with disordered alloys and the LDA+U [33] or DMFT [34, 114] to account for correlation effects beyond LSDA – as long as the latter schemes are used on a site-diagonal, i.e. single-site level.

In spite of the great success of the CPA many more sophisticated schemes have been worked out in the past to avoid the single-site approximation and to include SRO effects directly within

the primary electronic structure calculation [14]. Recently, a cluster extension of the single-site CPA – called non-local CPA (NL-CPA) – was suggested that is based on ideas borrowed from averaging techniques developed in many body theory [115, 116]. As Fig. 7 shows the basic idea of the NL-CPA is very similar to that of the CPA: embedding a cluster with given atomic configuration into the NL-CPA medium should not change its properties if the average over all possible configurations of the cluster is taken. Within multiple scattering formalism this can be

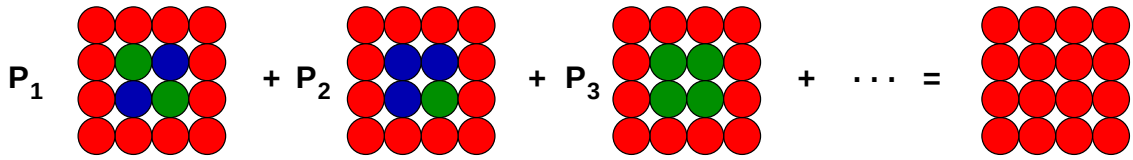

Figure 7: Basic idea of the non-local CPA (NL-CPA): embedding a cluster with given atomic configuration into the NL-CPA medium should not change its properties if the average over all possible configurations of the cluster is taken.

expressed again by the corresponding scattering path operators:

$$\sum_{\text{config } \gamma} P_\gamma \underline{\underline{\tau}}_\gamma = \underline{\underline{\tau}}^{\text{NL-CPA}} \,, \tag{18}$$

where the site index of the matrices runs over all sites within the cluster. The summation in Eq. (18) is performed over all possible atomic configurations γ of the cluster with the probability P_γ. For a completely disordered system the probabilities P_γ are all the same, but they differ if ordering or clustering occurs.

Fig. 8 shows results for the spin and orbital magnetic moment of Pt in disordered fcc-$Fe_{0.5}Pt_{0.5}$ as obtained by the NL-CPA [117]. For these calculations clusters with $N_c = 4$ atoms on the

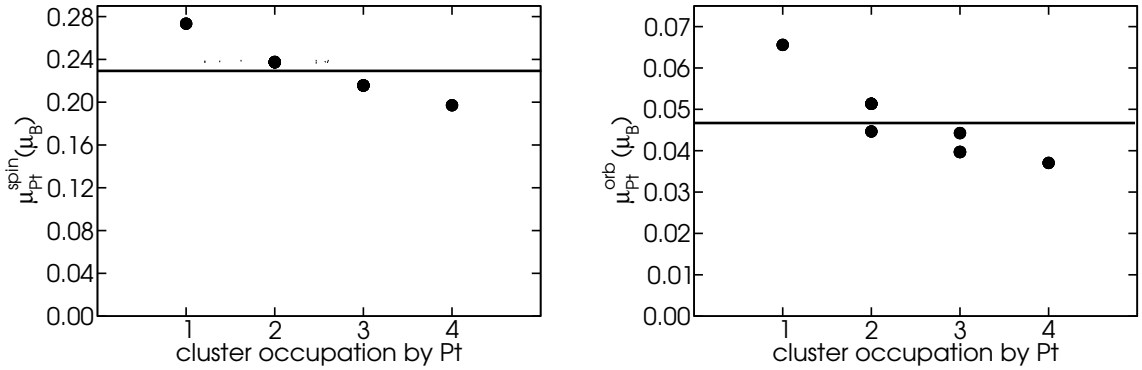

Figure 8: Spin (left) and orbital (right) magnetic moment of Pt in fcc-$Fe_{0.5}Pt_{0.5}$ as obtained by the NLCPA. The various data points show the moments for individual sites of all occurring cluster configurations for $N_c = 4$ as a function of the occupation of the cluster by Fe and Pt atoms, respectively. The horizontal lines represent the average NLCPA result, that nearly coincides with the CPA result [117].

fcc-lattice have been used; i.e. 2^4 configurations have been considered. The various data points give the moments as a function of the number of Pt atoms within the cluster (1-4). One notes that the induced Pt spin moment increases if the number of Fe atoms in the cluster increases (from the right to the left). For the spin moment obviously only the number of Fe atoms in

the cluster matters, i.e. the specific geometrical arrangement of the atoms within the cluster is more or less unimportant. For the orbital magnetic moment, on the other hand, that is very sensitive to the electronic structure at the Fermi level, the specific geometry matters as well as it is reflected by finding different moments for a given number of Fe atoms in the cluster.

There are already several further developments based on the NL-CPA and interesting corresponding applications to be found in the literature that demonstrate the great potential of this new scheme [116, 118, 119] (see also below).

7.7.1 Magnetic Anisotropy and Exchange interaction

Magnetic anisotropy denotes the dependency of the total energy of a system on the orientation of its magnetisation. For transition metal systems the magnetic anisotropy energy is usually split into a contribution, connected with the spin-orbit coupling and one associated with the dipole-dipole interaction of the individual magnetic moments [120, 121]. The latter one $\Delta E_{\rm dip}(\hat{n}, \hat{n}\,')$ is treated classically by evaluating a corresponding Madelung sum [121, 122]. The magnetic anisotropy energy $\Delta E_{\rm SOC}(\hat{n}, \hat{n}\,')$ connected with spin-orbit coupling, on the other hand, is determined by total energy calculations with the magnetisation oriented along directions $\hat{n}$ and $\hat{n}\,'$, respectively, and taking the difference. Obviously, for both orientations a full SCF calculation has to be performed. This can be avoided by making use of the so-called magnetic force theorem that allows to approximate $\Delta E_{\rm SOC}(\hat{n}, \hat{n}\,')$ by the difference of the single particle or band energies for the two orientations obtained using a frozen spin dependent potential [120]. This simple scheme has been used among other things for surface layered systems. In particular for $\mathrm{Fe}_n/\mathrm{Au}(001)$ it was found that the spin-orbit coupling term $\Delta E_{\rm SOC}(\hat{n}, \hat{n}\,')$ and the dipole-dipole term $\Delta E_{\rm dip}(\hat{n}, \hat{n}\,')$ are of the same order of magnitude leading to a change from out-of-plane to in-plane anisotropy if the number n of Fe layers is increased above three [121]. By decomposing the band-energy via the DOS in a layer-resolved way the anisotropy energy $\Delta E_{\rm SOC}(\hat{n}, \hat{n}\,')$ could be decomposed accordingly [123]. A corresponding analysis of $\Delta E_{\rm SOC}(\hat{n}, \hat{n}\,')$ shows in general that the dominating contributions originate from interface or surface layers, respectively.

An alternative to the calculation of $\Delta E_{\rm SOC}(\hat{n}, \hat{n}\,')$ via the total energy or the force theorem is to consider the torque exerted on a magnetic moment when the magnetisation is tilted away from its equilibrium orientation (easy axis). Using multiple scatting theory the torque component with respect to a rotation of the magnetisation about an axis $\hat{u}$ can be expressed as [124]:

$$T^{\hat{n}}_{\alpha^{\hat{u}}} = -\frac{1}{\pi}\,\Im \int^{E_F} dE\; \frac{\partial}{\partial \alpha^{\hat{u}}} \left[\ln\det\left(\underline{\underline{t}}(\hat{n})^{-1} - \underline{\underline{G}}^0\right)\right] \;. \tag{19}$$

The great flexibility of this approach has been demonstrated by investigations on the temperature dependence of the magnetic anisotropy energy of $\mathrm{L1_1}$-ordered FePt alloys [125]. Another example for its application are investigations on small deposited Fe clusters on a Pt(111) substrate [126]. Calculating the magnetic moments and anisotropy energies for various cluster sizes, the input necessary to simulate the magnetisation curves $M(B)$ for ensembles of Fe clusters could be supplied. Fig. 9 shows the results for two different temperatures compared with experimental data [126]. Obviously, the calculations based on Eq. (19) lead to a parameter set that is in very satisfying accordance with experiment.

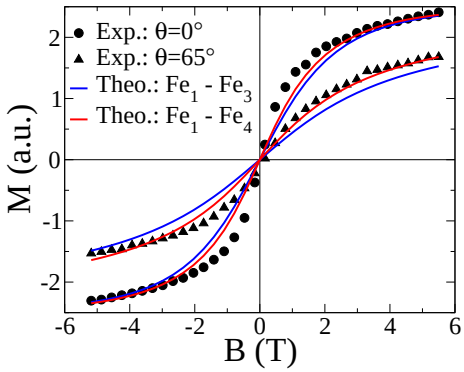

Figure 9: Experimental magnetisation curves $M(B)$ (dots) of an ensemble of Fe_n (n=1,2,3) clusters on Pt(111) measured at $T = 6$ K for an orientation of the magnetic field $M(B)$ along the easy axis $\hat{z}(\theta = 0°)$ and rotated by $\theta = 65°$ with respect to that. The full lines give corresponding theoretical results obtained on the basis of the calculated properties of Fe_n clusters and the Langevin formula. The dashed line is obtained by including in addition Fe_4 clusters in the simulation [126].

The expression for the magnetic torque given above is derived by considering the change of the single-particle energies if all magnetic moments change their orientations the same way. If only two moments change their relative orientation the corresponding change in the energy ΔE_{ij} can be expressed in an analogous way. As was shown by Lichtenstein et al. ΔE_{ij} can be expressed very elegantly within multiple scattering theory by making use of Lloyd's formula [51]. If ΔE_{ij} is expressed to lowest order with respect to the orientation angle of the moments $\hat{m}_i$ and $\hat{m}_j$, one gets a one-to-one mapping of the exchange coupling energy ΔE_{ij} to the Heisenberg Hamiltonian $\mathcal{H} = -\sum_{ij} J_{ij}\, \hat{m}_i \cdot \hat{m}_j$, with the coupling constants J_{ij} given by [51]:

$$J_{ij} = -\frac{1}{4\pi}\ Im \int^{E_F} dE\ \mathrm{Trace}\left(t_{i\uparrow}^{-1} - t_{i\downarrow}^{-1}\right) \tau_{\uparrow}^{ij} \left(t_{j\uparrow}^{-1} - t_{j\downarrow}^{-1}\right) \tau_{\downarrow}^{ji}\ . \tag{20}$$

This expression for the isotropic exchange coupling has been used extensively to supply the input for subsequent Monte-Carlo simulations on the basis of the Heisenberg Hamiltonian. This hybrid approach offers a realistic route to investigate magnetic properties at finite temperatures and has been applied with great success for bulk [127–129], layered [130–132], one-dimensional [133] as well as finite cluster systems [134, 135].

If spin-orbit coupling is accounted for the exchange coupling parameter in the Heisenberg Hamiltonian has to be replaced by a corresponding tensor:

$$\mathcal{H} = -\sum_{i\neq j} \hat{m}_i \underline{\underline{J}}_{ij} \hat{m}_j + \sum_i K(\hat{m}_i) \tag{21}$$

$$= -\sum_{i\neq j} J_{ij} \hat{m}_i \cdot \hat{m}_j - \sum_{i\neq j} \hat{m}_i \underline{\underline{J}}^{\mathrm{S}}_{ij} \hat{m}_j - \sum_{i\neq j} \vec{D}_{ij} \cdot (\hat{m}_i \times \hat{m}_j) + \sum_i K_i(\hat{m}_i)\ . \tag{22}$$

with the single-site magnetic anisotropy represented by the term $K(\hat{m}_i)$. In Eq. (22) the coupling tensor $\underline{\underline{J}}_{ij}$ has been decomposed in the standard way into its isotropic part J_{ij}, its traceless symmetric part $\underline{\underline{J}}^{\mathrm{S}}_{ij}$ and its anti-symmetric part that in turn is represented in terms of the so-called Dzyaloshinsky-Moriya (DM) vector $\vec{D}_{ij}$. A corresponding generalisation of the non-relativistic expression forJ_{ij} given in Eq. (20) to its relativistic tensor form was worked out by

Udvardi et al. [136]. An alternative expression, that offers several advantages, is given by [137]:

$$J_{ij}^{\alpha_i\alpha_j} = -\frac{1}{\pi}\Im\int dE\,\mathrm{Trace}\,\Delta\underline{V}^{\alpha_i}\,\underline{\tau}^{ij}\,\Delta\underline{V}^{\alpha_j}\,\underline{\tau}^{ji}\,, \tag{23}$$

with

$$\Delta V_{\Lambda\Lambda'}^{\alpha_i} = \int d^3r\,Z_{\Lambda}^{\times}(\vec{r})\,\beta\,\sigma_\alpha B(r)\,Z_{\Lambda'}(\vec{r})\,. \tag{24}$$

The expressions given above have been applied recently to a number of cluster systems [138,139] with the interest focussing on the impact of the DM-interaction. For Fe, Co, and Ni dimers on Pt(111) it was found for example that the DM-interaction leads to a tilting of the individual magnetic moments in the dimer in spite of the pronounced out-of-plane anisotropy and a strong ferromagnetic isotropic exchange coupling. Another system studied was an FePt cluster on Pt(111) that has rows of Fe atoms separated by Pt atoms (see Fig. 10). The left panel of Fig. 10

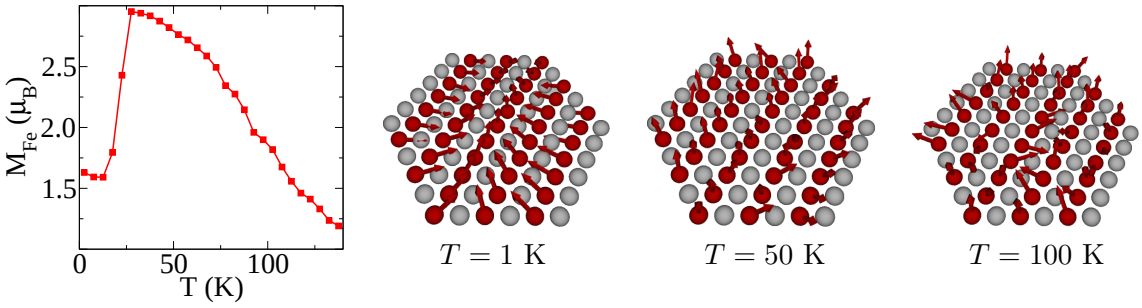

Figure 10: Left: Temperature dependence of the thermally averaged Fe moment $m_{\mathrm{Fe}}(T)$. Around $T = 25$ K the transition from non-collinear low-temperature structure caused by the Dzyaloshinsky-Moriya interaction to the ordered ferromagnetic structure occurs. Right: Magnetic structure of $Fe_{43}Pt_{48}$ cluster for three different temperature range: non-collinear ($T = 1$ K), ferromagnetic ($T = 50$ K) and disordered paramagnetic ($T = 100$ K) [139].

shows the thermally averaged Fe moment $m_{\mathrm{Fe}}(T)$ as a function of the temperature T that was obtained from Monte-Carlo simulations on the basis of the generalised Heisenberg Hamiltonian in Eq. (21). For high temperatures, one starts in the paramagnetic regime with the individual moments randomly oriented as it is shown by the snapshot for $T = 100$ K. With decreasing temperature the strong isotropic exchange coupling leads to a ferromagnetic alignment of the moments within each Fe row (see snapshot for $T = 50$ K). Below around $T = 25$ K the Fe-rows get coupled with their average moment tilted against each other due to the DM-interaction.

It should be emphasised that Eq. (21) is an approximate mapping of the complicated energy landscape $E(\{\hat{m}_i\})$ of a system calculated in an ab-initio way onto a simplified analytical expression. This implies corresponding limitations [138] in particular due to the use of the rigid spin approximation (RSA) [140]. A coupling tensor of the same shape as in Eq. (21) occurs for the indirect coupling of nuclear spins mediated by conduction electrons. In this case the above mentioned restrictions do not apply. As a consequence the linear response formalism on the basis of the Dyson equation can be used without restrictions to determine the corresponding nuclear spin – nuclear spin coupling tensor [141].

7.7.2 Magnetic response functions

The Green's function formalism supplies a natural basis for investigations on the response of a system to an external perturbation via the Dyson equation (10). Inserting the Dyson equation repeatedly into itself one obtains for the Green's function G^{pert} of the perturbed system a power series with respect to the perturbation $\mathcal{H}_{\mathrm{pert}}$ expressed in terms of the Green's function G^{ref} of the unperturbed reference system. Keeping only the first order term one ends up with the linear response of the system to the perturbation:

$$G^{\mathrm{pert}}(\vec{r},\vec{r}\,',E) = G^{\mathrm{ref}}(\vec{r},\vec{r}\,',E) + \int_{\Omega_{\mathrm{pert}}} d^3r''\, G^{\mathrm{ref}}(\vec{r},\vec{r}\,'',E)\, \mathcal{H}_{\mathrm{pert}}(\vec{r}\,'')\, G^{\mathrm{ref}}(\vec{r}\,'',\vec{r}\,',E)\ . \tag{25}$$

Considering for example the perturbation caused by a static magnetic field B_{ext} along the z-axis the corresponding perturbation $\mathcal{H}_{\mathrm{pert}}(\vec{r})$ may be written as:

$$\mathcal{H}_{\mathrm{pert}}(\vec{r}) = \underbrace{\beta\sigma_{\mathrm{z}}\,\mu_{\mathrm{B}}B_{\mathrm{ext}} + \beta\hat{l}_{\mathrm{z}}\,\mu_{\mathrm{B}}B_{\mathrm{ext}}}_{\text{Zeeman}} + \underbrace{\Delta V^{\mathrm{xc}}(\vec{r}) + \Delta V^{\mathrm{H}}(\vec{r})}_{\text{induced}}\ . \tag{26}$$

Here a relativistic formulation has been adopted with β standing for one of the standard Dirac matrices. The first two terms represent the Zeeman-type coupling of the external magnetic field to the spin and orbital angular momentum of the electrons, while the remaining terms represent the changes of the exchange-correlation (xc) and Hartree (H) potential induced by the perturbation. For non-magnetic solids the last term can usually be ignored. Focusing in this case on the spin magnetisation $m_{\mathrm{spin}}(\vec{r})$ induced by B_{ext} the second term can also be omitted if the influence of the spin-orbit coupling is neglected. Expressing now $m_{\mathrm{spin}}(\vec{r})$ as well as $\Delta V^{\mathrm{xc}}(\vec{r})$ in terms of $G^{\mathrm{pert}}(\vec{r},\vec{r}\,',E)$ using Eq. (26) one ends up with an implicit equation for $m_{\mathrm{spin}}(\vec{r})$ that in turn is linear with respect to B_{ext}. Accordingly, one gets a corresponding equation for the spin susceptibility χ_{spin} with the term connected with $\Delta V^{\mathrm{xc}}(\vec{r})$ giving rise to the Stoner-enhancement. This scheme was used to arrive at a formulation for the Stoner-enhanced spin susceptibility that accounts for the influence of spin-orbit coupling and that is applicable also for disordered alloys [142]. Later it was extended to include also orbital contributions giving rise to the Van-Vleck-susceptibility χ_{VV} as well as spin-orbit cross-terms [143]. In an analogous way the NMR Knight-shift in metals was formulated accounting for all spin and orbital contributions [144].

Dealing with spontaneously magnetised solids the last term in Eq. (26) has also to be included. In addition the Fermi energy may be shifted due to the perturbation. Including these modifications gives access to the high-field susceptibility χ_{HF} of ferromagnetic solids [145]. In Fig. 11 results of corresponding calculations for the alloy system bcc-$\mathrm{Co}_x\mathrm{Fe}_{1-x}$ are shown. For the Fe-rich regime of the system the experimental data are obviously reproduced quite well by the theoretical results. For the region around $x = 1/2$ agreement is less satisfying. However, accounting for partial ordering in the system in this regime, that may be expected because the equilibrium structure for $x = 1/2$ is the CsCl-structure, agreement between theory and experiment is again very good. The right panel of Fig. 11 shows the contribution of the spin susceptibility to the total high-field susceptibility of bcc-$\mathrm{Co}_x\mathrm{Fe}_{1-x}$. As one notes, the partial susceptibilities of Fe and Co are quite different and give rise to the concentration dependence of the total susceptibility (left panel). In addition one can see that the spin susceptibility is only a minor contribution to the total susceptibility that is dominated by its orbital Van-Vleck-contribution. The latter one

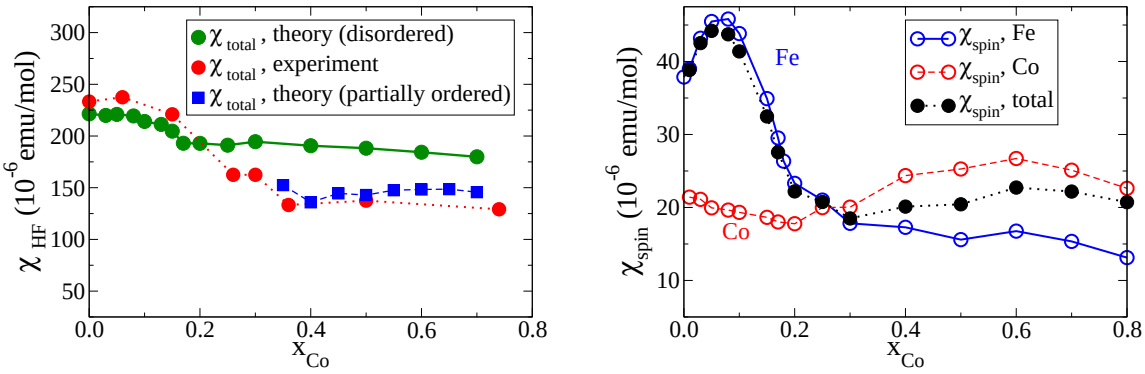

Figure 11: High-field magnetic susceptibility $\chi_{\rm HF}$ of bcc $Fe_{1-x}Co_x$ alloys: Total susceptibility (left); green circles correspond to randomly disordered alloys, while blue squares correspond to 'partially ordered' alloys. Experimental data are given by filled circles; (right) Element-resolved contributions to the spin magnetic susceptibility $\chi_{\rm spin}$ of Fe and Co in disordered $Fe_{1-x}Co_x$ [145].

is more or less concentration independent and is accompanied by an appreciable Landau-type contribution $\chi_{\rm Lan}$. Here, it should be noted that $\mathcal{H}_{\rm pert}$ given in Eq. (26) does not give access to $\chi_{\rm Lan}$. However, as was shown by Benkowitsch and Winter [146] for the non-relativistic case, $\chi_{\rm Lan}$ can be determined by starting from a spatially oscillating magnetic field $\vec{B}_{\vec{q}}(\vec{r})$ and considering the coupling of the orbital current density to the corresponding magnetic vector potential $\vec{A}_{\vec{q}}(\vec{r})$. A corresponding relativistic formulation suitable for magnetic solids was used to calculate $\chi_{\rm Lan}$ included in the total high-field susceptibility $\chi_{\rm HF}$ given in Fig. 11.

The formalism sketched here is not restricted to a static perturbation. Corresponding work on the frequency and wave-vector dependent dynamic spin susceptibility has been done for example on pure Pd on a non-relativistic level [147].

7.7.3 Transport properties

Another important field for the application of linear response formalism is electronic transport. As mentioned above, Butler and Stocks demonstrated the use of the KKR-GF-CPA to calculate the residual resistivity of disordered alloys on the basis of the Boltzmann formalism [98]. Later on an expression for the electronic conductivity of alloys was developed by Butler on the basis of the Kubo-Greenwood formalism and the KKR-GF-CPA that allows to express the elements of the symmetric conductivity tensor $\underline{\underline{\sigma}}$ in terms of the auxilary conductivities $\tilde{\sigma}_{\mu\nu}$ [148]:

$$\tilde{\sigma}_{\mu\nu} = -\frac{4m^2}{\pi\hbar^3\Omega}\left(\sum_{\alpha,\beta}\sum_{\substack{L_1,L_2\\L_3,L_4}} x_\alpha x_\beta \tilde{J}^{\alpha\mu}_{L_4,L_1}(z_2,z_1)\Big[\{1-\chi\omega\}^{-1}\chi\Big]_{\substack{L_1,L_2\\L_3,L_4}} \tilde{J}^{\beta\nu}_{L_2,L_3}(z_1,z_2) + \sum_{\alpha}\sum_{\substack{L_1,L_2\\L_3,L_4}} x_\alpha \tilde{J}^{\alpha\mu}_{L_4,L_1}(z_2,z_1)\tau^{\rm CPA\,00}_{L_1,L_2}(z_1)J^{\alpha\nu}_{L_2,L_3}(z_1,z_2)\tau^{\rm CPA\,00}_{L_3,L_4}(z_2)\right), \qquad (27)$$

with $z_{1(2)} = E_{\rm F} \pm i\epsilon$. Here the quantities $J^{\alpha\mu}_{LL'}$ are matrix elements of the μ-component of the current density operator $\vec{j}$ for the alloy component α, with $\tilde{J}^{\alpha\mu}$ involving in addition the component projected scattering path operators $\underline{\tau}^{\alpha}$. The term χ stands for a sum over all

scattering path operators $\tau^{\mathrm{CPA}\,0n}_{L,L'}(z_1)\tau^{\mathrm{CPA}\,n0}_{L'',L'''}(z_2)$ with $n \neq 0$ and the expression in curly bracket accounts for the so-called vertex corrections.

Results of a corresponding application to disordered $\mathrm{Ag}_x\mathrm{Pd}_{1-x}$ are shown in Fig. 12 [149]. The

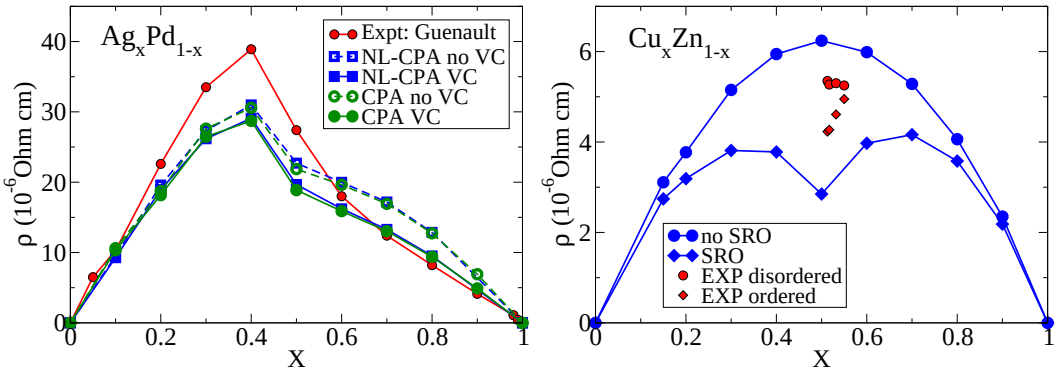

Figure 12: Left: Residual resistivity in disordered $\mathrm{Ag}_x\mathrm{Pd}_{1-x}$ alloys as a function of the concentration x. Results are shown obtained on the basis of the CPA and NL-CPA including (VC) and excluding (no VC) the vertex corrections. Experimental results are shown in addition. Right: Residual resistivity in disordered bcc-$\mathrm{Cu}_x\mathrm{Zn}_{1-x}$ alloys as a function of the concentration obtained using the NL-CPA. Results are shown including (SRO) and excluding (no SRO) atomic short-range order together with corresponding experimental data [149].

calculations have been performed with and without inclusion of the so-called vertex corrections. As one notes these have an impact on the residual resistivity only on the Ag-rich side of the alloy system. In addition, one finds that the experimental data are reproduced quite well by the calculations implying in particular that the single-site CPA is completely sufficient to deal with the residual resistivity of randomly disordered alloys. This is also confirmed by calculations based on the NL-CPA formalism [149]. As Fig. 12 shows corresponding results are indeed in very good agreement with the resistivity obtained by using the CPA.

In addition, Fig. 12 shows the residual resistivity in disordered bcc-$\mathrm{Cu}_x\mathrm{Zn}_{1-x}$ alloys as a function of the concentration obtained using the NL-CPA including the vertex corrections [149]. Assuming a random distribution of the alloy components a simple parabolic variation of the resistivity with concentration is found. On the other hand, assuming SRO according to the CsCl-structure within the NL-CPA cluster a pronounced reduction in the resistivity is found as it is expected from the corresponding experimental data that are also shown in Fig. 12.

The scheme to implement the Kubo-Greenwood (KG) equation for disordered alloys sketched above (see Eq. (27)), can also be used to introduce a layer-resolved conductivity $\sigma^{II'}$ appropriate for two-dimensional periodic systems [150–152], with I and I' being layer indices. This approach was later extended to finite frequencies [153, 154] supplying a suitable basis for investigations on the spin-orbit induced magneto-optical Kerr-effect of magnetic surface layer systems [153, 155, 156], that can show a pronounced enhancement of the Kerr rotation as a function of the layer thickness. As an alternative to the Kubo-Greenwood formalism, transport in two-dimensional systems may also be described in terms of a layer-resolved conductance $g^{II'}$ introduced within the framework of the Landauer-Büttiker (LB) formalism [157, 158]:

$$g^{II'} \propto \int d\vec{k}_{\parallel} \sum_{\substack{n\in I \\ n'\in I'}} \mathrm{Trace}\left[\underline{J}^{n}\,\underline{G}^{nn'}(\vec{k}_{\parallel}, E_{\mathrm{F}})\,\underline{J}^{n'}\,\underline{G}^{nn'\dagger}(\vec{k}_{\parallel}, E_{\mathrm{F}})\right] , \tag{28}$$

with the matrix elements of the perpendicular component of the current density operator $\vec{j}$:

$$J^n_{\Lambda\Lambda'} = \frac{1}{V_n}\int_{S_n} d^2r R^{n\times}_{\Lambda}\, j_\perp\, a_\perp\, R^n_{\Lambda'}\ . \tag{29}$$

The Kubo-Greenwood and Landauer-Büttiker approaches have been used extensively to investigate the giant magneto resistance (GMR) [159–161] and the tunnelling magneto resistance (TMR) [162–165] of FM/SP/FM trilayer systems consisting of ferromagnetic (FM) leads separated by a non-magnetic metallic or insulating, respectively, spacer (SP). Corresponding studies were dealing among other with the influence of the relative orientation of the magnetisation in the magnetic leads [160, 166] or spin-flip processes due to spin-orbit coupling [165]. Corresponding results of relativistic calculations for the conductance g of the trilayer system Fe/n(GaAs)/Fe with Ga-termination are shown in Fig. 13 [165] for the magnetisation in ([110]) and out-off ([001]) plane. Although for both geometries the magnetisation of the magnetic leads are parallel, there

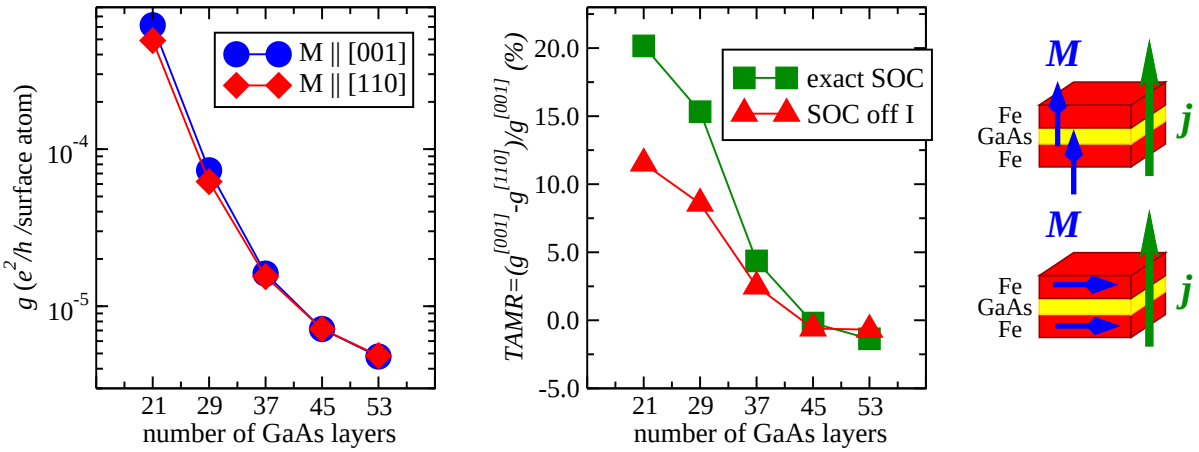

Figure 13: Left: conductance g of the trilayer system Fe/n(GaAs)/Fe with Ga-termination for the magnetisation in ([110]) and out-off ([001]) plane. Right: sketch for the in (bottom) and out-off (top) plane geometry. Middle: first type of tunnelling anisotropic magneto resistance (TAMR) for the full spin-orbit coupling (exact SOC) and for the spin-orbit coupling suppressed for the interface layers (SOC off I).

is a pronounced dependence of the conductance on the orientation of the magnetisation due to spin-orbit coupling. The middle panel of Fig. 13 shows that the corresponding tunnelling anisotropic magneto resistance (TAMR) can be as large as 200 % for a thin GaAs-spacer. The fact that the TAMR is caused by spin-orbit coupling can be demonstrated very easily. In addition to the TAMR for the full spin-orbit coupling (exact SOC) results for the spin-orbit coupling suppressed for the interface layers (SOC off I) are shown in addition in the middle panel of Fig. 13. The drop of the TAMR by nearly a factor 2 reflects the central role of the hybridisation at the Fe/GaAs-interface for the TAMR. This gets even more important for a second type of TAMR that can be observed even with only one magnetic layer present [167]. Fig. 14 shows the corresponding set up for a Fe/(GaAs)/Au trilayer system with the magnetisation of the Fe lead in plane. Rotating the magnetisation in the plane changes the hybridisation at the interface due to spin-orbit coupling and gives rise to a corresponding variation of the conductance with the rotation angle. As Fig. 14 shows, the experimental results [167] for this second type of TAMR are reasonably well reproduced by the calculations [168]. Again the central role of spin-orbit

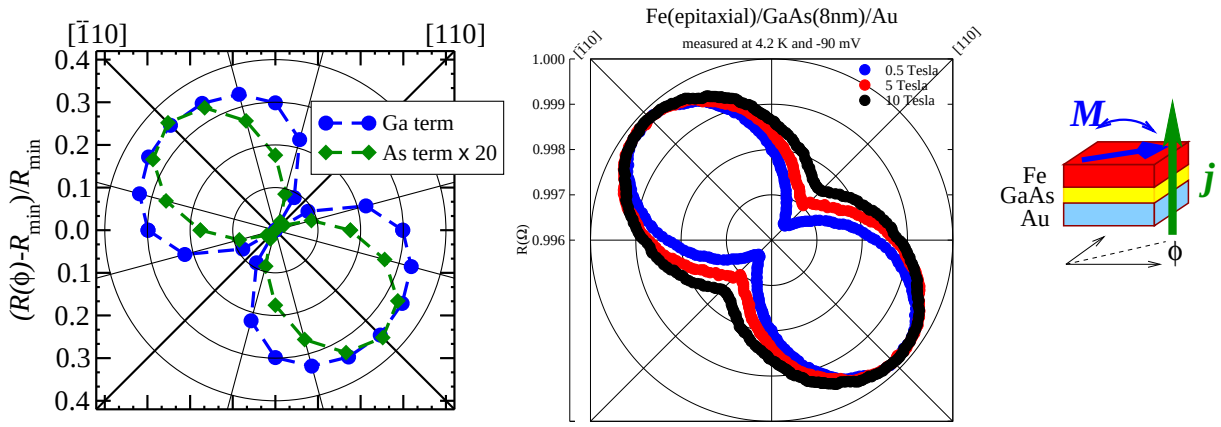

Figure 14: Left: theoretical results for the second type of TAMR in Ga and As terminated Fe/29(GaAs)/Au. Middle: corresponding experimental results for Fe/GaAs(8nm)/Au. Right: sketch of the geometry.

coupling can easily be demonstrated by model calculations with the strength of the spin-orbit coupling manipulated.

The transport theory for layered systems presented above can be applied more or less directly to lead/wire/lead systems. Corresponding investigations accounted in particular for the influence of spin-orbit coupling and a non-collinear spin configuration within the wire [82]. The effect of a finite bias voltage on the TAMR was already investigated using the sketched linear response schemes [164]. A more general description can be achieved by use of the steady state Keldysh or non-equilibrium Green's function approach. A first implementation of this numerically quite demanding scheme within the KKR-GF formalism could already be presented [169, 170].

7.7.4 Electron Spectroscopy

When dealing with electron spectroscopies multiple scattering theory offers especially great advantages compared to any other scheme for electronic structure calculations. A most prominent example is EXAFS (extended X-ray absorption fine structure) [171]. An adequate theoretical description has to deal with matrix elements with respect to the electron-photon interaction operator with a tightly bound core state and an extended final state involved. As the final state lies in the energy range of about 50 – 1500 eV above the Fermi level, the energy-dependence of the final state wave function cannot be ignored. For the same reason non-dipole contributions to the matrix element may become important. The finite life time of the final state caused by various relaxation processes is usually accounted for by a corresponding complex and energy dependent self-energy $\Sigma(E)$ [172]. Finally, the influence of the environment of the absorber atom on its electronic structure has to be included in a transparent way – again up to very high energies. All these requirements are met by applying multiple scattering theory to a finite cluster centred at the absorber atom. In particular a connection of the oscillations observed in an EXAFS spectrum and the atomic configuration around the absorber atom can be established in a transparent way. A similar situation occurs for many other core level spectroscopies [39, 40, 173, 174].

In the case of a crystalline solid most detailed information on its electronic structure can be

obtained by use of angle-resolved photo emission spectroscopy (ARPES) applied to the valence band. An appropriate theoretical description of ARPES is supplied by the so-called one-step model of photo emission that expresses the photo electron current $j^{\vec{q}\lambda}_{\vec{k}m_s}(E_\mathrm{f})$ by making use of Fermi's golden rule [56, 175–177]:

$$j^{\vec{q}\lambda}_{\vec{k}m_s}(E_\mathrm{f}) \;\propto\; \Im \int d^3r \int d^3r' \left[\mathcal{T}\,\phi^{\mathrm{LEED}}_{\vec{k}m_s}(\vec{r},E_\mathrm{f})\right]^\dagger X_{\vec{q}\lambda}(\vec{r}) \\ G(\vec{r},\vec{r}\,',E_\mathrm{i})\, X^\dagger_{\vec{q}\lambda}(\vec{r}\,')\,\mathcal{T}\,\phi^{\mathrm{LEED}}_{\vec{k}m_s}(\vec{r}\,',E_\mathrm{f}) \qquad (30)$$

with

$$\phi^{\mathrm{LEED}}_{\vec{k}m_s}(\vec{r},E_\mathrm{f}) \;=\; \Xi_{m_s} e^{i\vec{k}\vec{r}} + \int d^3r'\, G(\vec{r},\vec{r}\,',E_\mathrm{f})\, V(\vec{r}\,')\, \Xi_{m_s} e^{i\vec{k}\vec{r}\,'}\;. \qquad (31)$$

Here the initial valence band states at energy E_i are represented by the Green's function $G(E_\mathrm{i})$. The final state at energy $E_\mathrm{f} = E_\mathrm{i} + \hbar\omega$ – a so-called time-reversed LEED-state – is constructed on the basis of the Lippmann-Schwinger-equation involving the Green's function at energy E_f, Ξ_{m_s} represents the spin part of the free-electron wave function charcaterized by the quantum number m_s and $\mathcal{T}$ is the time reversal operator. Finally, $X_{\vec{q}\lambda}(\vec{r})$ is the electron-photon interaction operator for radiation with wave vector $\vec{q}$ and polarisation λ.

Again evaluating the expression for the photo electron current by means of multiple scattering theory allows to account in an appropriate way for matrix-elements, finite life time effects represented by a corresponding self-energy $\Sigma(E)$ and – most important in the UV-regime – for the surface of the system. This allows in particular for a proper inclusion of contributions to the photo electron current due to surface states. In fact, many experimental and theoretical investigations are focused recently on the influence of spin-orbit coupling giving rise to the so-called Rashba-splitting for the surface states [178, 179]. As for all other electronic properties disorder in the system may be accounted for by means of the CPA within an ARPES calculation based on multiple scattering theory [176, 180].

During the last one or two decades the resolution of ARPES experiments could be substantially improved allowing for a very detailed mapping of the electronic properties of solids. Results of a corresponding investigation on Ni(110) at a photon energy of $\hbar\omega = 21$ eV are shown in Fig. 15 and compared to the bulk spectral function calculated on the basis of the LSDA [181]. Obviously, the various features of the experimental spectra cannot be described in a satisfying way on that basis indicating the non-negligible influence of correlation effects not accounted for by LSDA. In fact, calculations of the spectral function on the basis of the LSDA+3BS (three body scattering) many-body formalism describe the spectra in a much better way [181], but still neglect the influence of matrix-elements and of the surface. Application of the KKR-GF-formalism, on the other hand, allowed to account for these on the basis of the one-step model of photo emission [182]. In addition, correlation effects were accounted for by making use of the LSDA+DMFT scheme [34]. As Fig. 15 shows this coherent approach leads to a very satisfying agreement of the calculated photo current and the experimental one.

During the last years ARPES experiments were continuously pushed to higher photon energies up to the keV-regime to reduce the surface sensitivity of this spectroscopy and to probe primarily the electronic structure of the bulk this way. Apart from many technical problems this raises

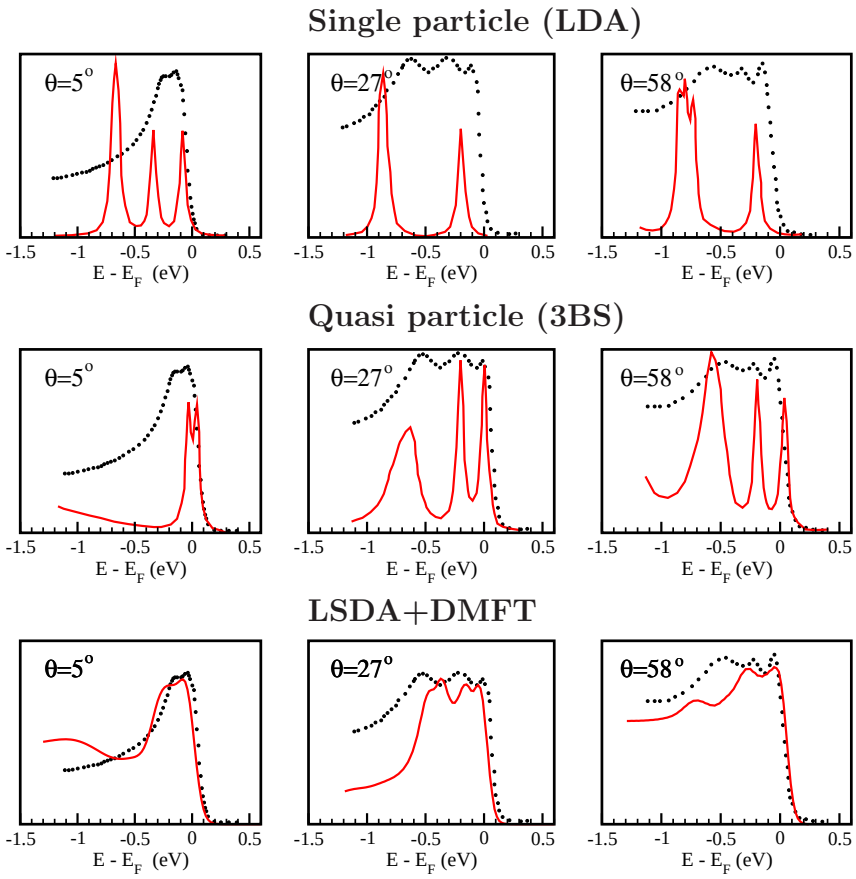

Figure 15: Spin-integrated ARPES spectra from Ni(011) along $\bar{\Gamma}$-$\bar{Y}$ for three different angles of emission. Upper row: comparison between LSDA-based calculations and experiment [181]; middle row: comparison between experiment and non-self-consistent quasi particle calculations neglecting matrix element and surface effects [181]; lower row: spin-integrated LSDA+DMFT spectra including photo emission matrix elements (this work). Theory: solid red line, experiment: black dots [182].

several questions concerning the interpretation of the ARPES spectra on the experimental side. Also for the calculation of ARPES spectra in the soft or hard X-ray regime extensions have to be introduced as the momentum of the photon cannot be neglected any more and non-dipole contributions may get important. Fig. 16 shows results of corresponding investigations on the ARPES of W(110) for a photon energy of $\hbar\omega = 260$ eV [183]. Obviously, the calculations based on the one-step model reproduce the experimental spectral data rather well. In addition, one notes that the spectra essentially follow the dispersion relation $E_{\vec{k}}$ calculated for bulk W rather well indicating that for the selected photon energy indeed primarily the bulk band structure is probed. The experimental data shown in Fig. 16 were recorded at $T = 300$ K. For higher temperatures but also for higher photon energies the influence of lattice vibrations gets more and more pronounced leading finally to spectra that essentially reflect the DOS of the system [183]. Theoretical schemes to deal with this complex situation have already been suggested [184] that should allow for corresponding calculations of the spectra in the near future.

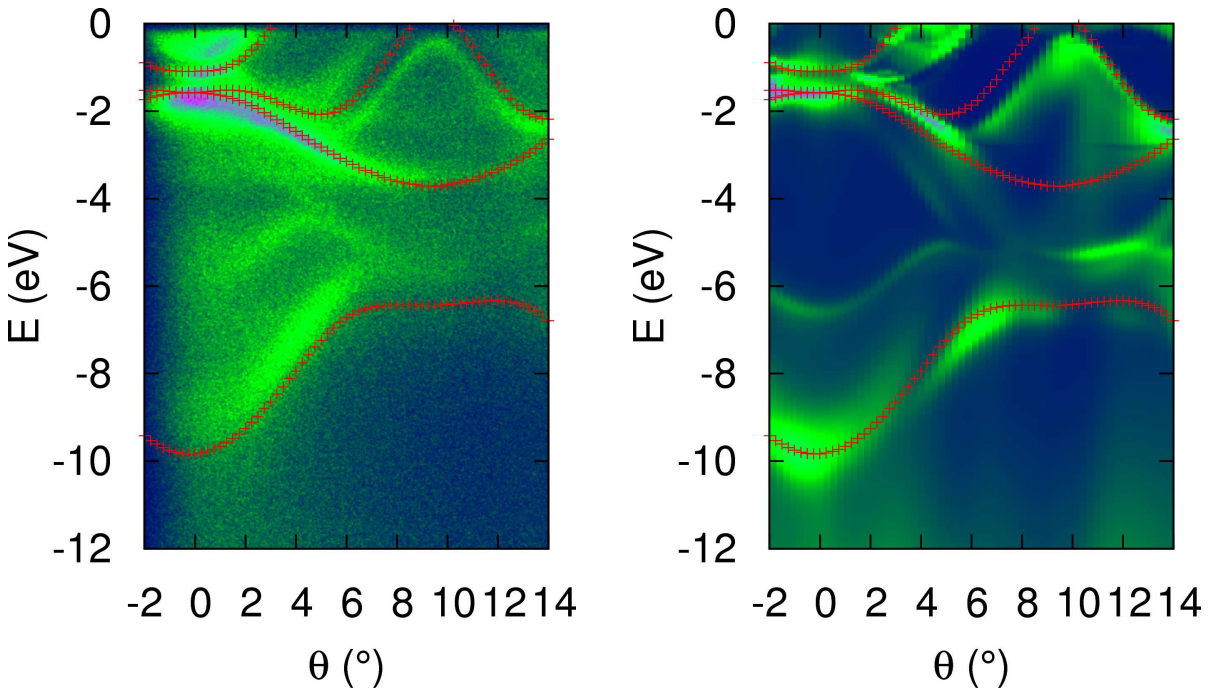

Figure 16: Plots of the experimental (left) and theoretical (right) photo current intensity for the excitation from the valence bands of W(110) at $T = 300$ K with a photon energy of $\hbar\omega = 260$ eV as a function of the initial state energy and the angle of emission with respect to the surface normal. The emission angle corresponds essentially to a probing of initial states with $\vec{k}$ along the Γ-to-N line in the Brillouin zone with a corresponding dispersion relation $E_{\vec{k}}$ included [183].

7.8 Concluding remarks

The various examples presented in some detail[7] were meant to demonstrate that the KKR-GF-method provides a very flexible framework to deal with a wide range of systems and properties using one and the same formalism without using unnecessary simplifications or artificial boundary conditions.[8] One of the reasons for the flexibility of the KKR-GF is the fact that it is an all-electron method using a minimal, numerical and energy-dependent basis set. This allows to deal, for example, with hyperfine interaction, EXAFS or valence band photo-emission accounting for all their specific features and to interpret the results in a chemically intuitive way. The most important feature, however, is that the KKR-GF supplies the electronic Green's function directly. This is of great advantage when dealing with spectroscopic properties or making contact with many-body schemes that go beyond LDA as in these cases representing the electronic structure in terms of the Green's function is the standard starting point. Connected with the availability of the Green's function is the use of the Dyson equation that can be exploited in many different ways. One branch is the description of complex systems on the basis of a simpler reference system. The other branch is the straight forward investigation of all type of response quantities. Finally, one should mention the treatment of disorder by means of the CPA or NL-CPA with their application not at all restricted to chemical disorder in alloys.

[7] In fact these reflect only some of the activities of the authors; i.e. much more examples can be found via the various references given, that are by no means complete ...

[8] This statement does not imply the claim that other methods are not able or useful to deal with the systems or properties considered here.

Of course, the various features of the KKR-GF method give also rise to some disadvantages. Solving the single-site problem for the full complexity of the underlying Hamiltonian, for example, implies accuracy but also corresponding numerical effort. This can be reduced, however, to a large extent by the Born series technique. Another more serious drawback is the use of fixed atomic positions for the reference system making atomic relaxation somewhat cumbersome. However, various techniques are available now that should allow to account for atomic relaxations more or less routinely. Obviously, these minor technical problems are more than outweighed by the many advantages offered by the KKR-GF method.

References

[1] J. Korringa, Physica **XIII**, 392 (1947).

[2] W. Kohn and N. Rostoker, Phys. Rev. **94**, 1111 (1954).

[3] A. R. Williams, S. M. Hu, and D. W. Jepsen, in *Computational Methods in Band Theory*, edited by P. M. Marcus, J. F. Janak, and A. R. Williams (Plenum, New York, 1971), p. 157.

[4] J. C. Slater and K. H. Johnson, Phys. Rev. B **5**, 844 (1972).

[5] A. R. Williams, J. F. Janak, and V. L. Moruzzi, Phys. Rev. B **6**, 4509 (1972).

[6] V. L. Moruzzi, J. F. Janak, and A. R. Williams, *Calculated Electronic Properties of Metals* (Pergamon, New York, 1978).

[7] O. K. Andersen, Phys. Rev. B **12**, 3060 (1975).

[8] J. L. Beeby, Proc. Roy. Soc. (London) A **302**, 113 (1967).

[9] J. Korringa, J. Phys. Chem. Solids **7**, 252 (1958).

[10] J. L. Beeby, Phys. Rev. **135**, A130 (1964).

[11] I. Turek *et al.*, *Electronic structure of disordered alloys, surfaces and interfaces* (Kluwer Academic Publ., Boston, 1997).

[12] L. V. Pourovskii *et al.*, Phys. Rev. B **71**, 94415 (2005).

[13] P. Weinberger, I. Turek, and L. Szunyogh, Intern. J. Quantum. Chem. **63**, 165 (1997).

[14] J. S. Faulkner, Prog. Mater. Sci. **27**, 3 (1982).

[15] W. H. Butler and R. K. Nesbet, Phys. Rev. B **42**, 1518 (1990).

[16] P. H. Dederichs, B. Drittler, and R. Zeller, Mat. Res. Soc. Symp. Proc. **253**, 185 (1992).

[17] W. H. Butler, A. Gonis, and X. G. Zhang, Phys. Rev. B **48**, 2118 (1993).

[18] M. Ogura and H. Akai, J. Phys.: Condensed Matter **17**, 5741 (2005).

[19] M. Ogura and H. Akai, J. Comp. Theo. Nanoscience **6**, 2483 (2009).

[20] T. Huhne *et al.*, Phys. Rev. B **58**, 10236 (1998).

[21] M. Czerner, B. Y. Yavorsky, and I. Mertig, J. Appl. Physics **103**, 07F304 (2008).

[22] S. Lounis, P. Mavropoulos, P. H. Dederichs, and S. Blügel, Phys. Rev. B **72**, 224437 (2005).

[23] A. Gonis and W. H. Butler, *Multiple scattering in solids*, *Graduate Texts in Contemporary Physics* (Springer, Berlin, 1999).

[24] J. B. Staunton, B. L. Györffy, and P. Weinberger, J. Phys. F: Met. Phys. **10**, 2665 (1980).

[25] M. E. Rose, *Relativistic Electron Theory* (Wiley, New York, 1961).

[26] R. Feder, F. Rosicky, and B. Ackermann, Z. Physik B **52**, 31 (1983).

[27] P. Strange, J. B. Staunton, and B. L. Györffy, J. Phys. C: Solid State Phys. **17**, 3355 (1984).

[28] H. Ebert, M. Battocletti, and E. K. U. Gross, Europhys. Lett. **40**, 545 (1997).

[29] H. Ebert, in *Electronic Structure and Physical Properties of Solids*, Vol. 535 of *Lecture Notes in Physics*, edited by H. Dreyssé (Springer, Berlin, 2000), p. 191.

[30] M. Lüders *et al.*, Phys. Rev. B **71**, 205109 (2005).

[31] M. Toyoda, H. Akai, K. Sato, and H. Katayama-Yoshida, Physica B **376-377**, 647 (2006).

[32] H. Ebert and M. Battocletti, Solid State Commun. **98**, 785 (1996).

[33] H. Ebert, A. Perlov, and S. Mankovsky, Solid State Commun. **127**, 443 (2003).

[34] J. Minár *et al.*, Phys. Rev. B **72**, 45125 (2005).

[35] H. Ebert, Phys. Rev. B **38**, 9390 (1988).

[36] B. C. H. Krutzen and F. Springelkamp, J. Phys.: Condensed Matter **1**, 8369 (1989).

[37] B. L. Györffy and M. J. Stott, in *Band Structure Spectroscopy of Metals and Alloys*, edited by D. J. Fabian and L. M. Watson (Academic Press, New York, 1973), p. 385.

[38] J. S. Faulkner, J. Phys. C: Solid State Phys. **10**, 4661 (1977).

[39] H. Ebert, V. Popescu, and D. Ahlers, Phys. Rev. B **60**, 7156 (1999).

[40] J. J. Rehr, J. Phys.: Condensed Matter **15**, S647 (2003).

[41] Y. Wang, G. M. Stocks, W. A. Shelton, and D. M. C. Nicholson, Phys. Rev. Letters **75**, 2867 (1995).

[42] Y. Onodera and M. Okazaki, J. Phys. Soc. Japan **21**, 1273 (1966).

[43] P. Lloyd and P. V. Smith, Adv. Phys. **21**, 69 (1972).

[44] P. Ziesche, J. Phys. C: Solid State Phys. **7**, 1085 (1974).

[45] R. Zeller, J. Phys.: Condensed Matter **17**, 5367 (2005).

[46] R. Zeller, J. Phys.: Condensed Matter **20**, 035220 (2008).

[47] A. F. Tatarchenko and N. I. Kulikov, Phys. Rev. B **50**, 8266 (1994).

[48] H. Akai and P. H. Dederichs, Phys. Rev. B **47**, 8739 (1993).

[49] B. Drittler, M. Weinert, R. Zeller, and P. H. Dederichs, Phys. Rev. B **39**, 930 (1989).

[50] T. Oguchi, K. Terakura, and N. Hamada, J. Phys. F: Met. Phys. **13**, 145 (1983).

[51] A. I. Liechtenstein, M. I. Katsnelson, V. P. Antropov, and V. A. Gubanov, J. Magn. Magn. Materials **67**, 65 (1987).

[52] H. L. Davis, in *Computational Methods in Band Theory*, edited by P. M. Marcus, J. F. Janak, and A. R. Williams (Plenum, New York, 1971), p. 183.

[53] K. Kambe, Z. Naturf. **22a**, 322 (1967).

[54] J. M. MacLaren, S. Crampin, D. D. Vvedensky, and J. B. Pendry, Phys. Rev. B **40**, 12164 (1989).

[55] J. B. Pendry, *Low energy electron diffraction* (Academic Press, London, 1974).

[56] J. Braun, Rep. Prog. Phys. **59**, 1267 (1996).

[57] T. Huhne and H. Ebert, Phys. Rev. B **65**, 205125 (2002).

[58] J. S. Faulkner and G. M. Stocks, Phys. Rev. B **21**, 3222 (1980).

[59] E. Tamura, Phys. Rev. B **45**, 3271 (1992).

[60] R. Zeller *et al.*, Phys. Rev. B **52**, 8807 (1995).

[61] E. N. Economou, *Green's Functions in Quantum Physics* (Springer-Verlag, New York, 1990).

[62] R. Zeller, J. Deutz, and P. H. Dederichs, Solid State Commun. **44**, 993 (1982).

[63] K. Wildberger, P. Lang, R. Zeller, and P. H. Dederichs, Phys. Rev. B **52**, 11502 (1995).

[64] H. Akai, J. Phys.: Condensed Matter **1**, 8045 (1989).

[65] L. Szunyogh, B. Újfalussy, P. Weinberger, and J. Kollar, Phys. Rev. B **49**, 2721 (1994).

[66] O. K. Andersen and O. Jepsen, Phys. Rev. Letters **53**, 2571 (1984).

[67] R. Zeller, J. Phys.: Condensed Matter **20**, 294215 (2008).

[68] B. Drittler, H. Ebert, R. Zeller, and P. H. Dederichs, Phys. Rev. B **39**, 6334 (1989).

[69] R. Zeller, Modelling Simul. Mater. Sci. Eng. **1**, 553 (1993).

[70] M. J. Puska and R. M. Nieminen, Rev. Mod. Phys. **66**, 841 (1994).

[71] V. S. Stepanyuk *et al.*, Phys. Rev. B **54**, 14121 (1996).

[72] B. Nonas, K. Wildberger, R. Zeller, and P. H. Dederichs, Phys. Rev. B **57**, 84 (1998).

[73] W. Hergert, V. S. Stepanyuk, R. Zeller, and P. H. Dederichs, J. Magn. Magn. Materials **198-199**, 233 (1999).

[74] O. O. Brovko, W. Hergert, and V. S. Stepanyuk, Phys. Rev. B **79**, 205426 (2009).

[75] S. Lounis, P. Mavropoulos, P. H. Dederichs, and S. Blügel, Phys. Rev. B **73**, 195421 (2006).

[76] V. S. Stepanyuk *et al.*, Phys. Rev. Letters **97**, 186403 (2006).

[77] V. S. Stepanyuk, L. Niebergall, W. Hergert, and P. Bruno, Phys. Rev. Letters **94**, 187201 (2005).

[78] K. Tao *et al.*, Phys. Rev. Letters **103**, 057202 (2009).

[79] S. Lounis, P. H. Dederichs, and S. Blügel, Phys. Rev. Letters **101**, 107204 (2008).

[80] V. S. Stepanyuk *et al.*, Phys. Rev. B **70**, 195420 (2004).

[81] M. Czerner *et al.*, Phys. Rev. B **74**, 115108 (2006).

[82] M. Czerner, B. Y. Yavorsky, and I. Mertig, Phys. Rev. B **77**, 104411 (2008).

[83] A. Lodder, J. Phys. F: Met. Phys. **6**, 1885 (1976).

[84] N. Papanikolaou, R. Zeller, P. H. Dederichs, and N. Stefanou, Phys. Rev. B **55**, 4157 (1997).

[85] S. K. Nayak, P. Jena, V. S. Stepanyuk, and W. Hergert, Surf. Sci. **491**, 219 (2001).

[86] A. Gonis, Phys. Rev. B **34**, 1290 (1986).

[87] P. M. Oppeneer and A. Lodder, J. Phys. F: Met. Phys. **17**, 1901 (1987).

[88] C. Zecha *et al.*, Hyperfine Interactions **158**, 59 (2005).

[89] C. Zecha, Ph.D. thesis, University of Munich, 2001.

[90] M. Takeda and H. Akai, to be published (2010).

[91] P. Soven, Phys. Rev. **156**, 809 (1967).

[92] B. L. Györffy, Phys. Rev. B **5**, 2382 (1972).

[93] B. Ginatempo and J. B. Staunton, J. Phys. F: Met. Phys. **18**, 1827 (1988).

[94] H. Akai *et al.*, Progr. Theor. Phys. Suppl. **101**, 11 (1990).

[95] H. Ebert, Rep. Prog. Phys. **59**, 1665 (1996).

[96] G. M. Stocks, W. M. Temmerman, and B. L. Györffy, Phys. Rev. Letters **41**, 339 (1978).

[97] H. Ebert, A. Vernes, and J. Banhart, Solid State Commun. **104**, 243 (1997).

[98] W. H. Butler and G. M. Stocks, Phys. Rev. Letters **48**, 55 (1982).

[99] J. Banhart and H. Ebert, Europhys. Lett. **32**, 517 (1995).

[100] A. Crepieux and P. Bruno, Phys. Rev. B **64**, 014416 (2001).

[101] B. L. Gyorffy and G. M. Stocks, Phys. Rev. Letters **50**, 374 (1983).

[102] A. Gonis, W. H. Butler, and G. M. Stocks, Phys. Rev. Letters **50**, 1482 (1983).

[103] J. Banhart, H. Ebert, J. Voitländer, and P. Weinberger, Solid State Commun. **65**, 693 (1988).

[104] H. Ebert *et al.*, Solid State Commun. **64**, 1011 (1987).

[105] J. M. MacLaren and R. H. Victora, J. Appl. Physics **76**, 6069 (1994).

[106] J. Minár and H. Ebert, Appl. Physics A: Mat. Science & Proc. **78**, 847 (2004).

[107] O. Šipr, J. Minár, J. Vackář, and H. Ebert, Phys. Rev. B **75**, 134422 (2007).

[108] V. Drchal *et al.*, Comp. Mater. Science **15**, 144 (1999).

[109] C. Etz *et al.*, Phys. Rev. B **75**, 245432 (2007).

[110] A. J. Pindor, J. Staunton, G. M. Stocks, and H. Winter, J. Phys. F: Met. Phys. **13**, 979 (1983).

[111] J. Staunton *et al.*, J. Magn. Magn. Materials **45**, 15 (1984).

[112] S. S. A. Razee, J. B. Staunton, L. Szunyogh, and B. L. Gyorffy, Phys. Rev. Letters **88**, 147201 (2002).

[113] I. D. Hughes *et al.*, Nature **443**, 650 (2007).

[114] V. Drchal, V. Janis, and J. Kudrnovský, Phys. Rev. B **60**, 15664 (1999).

[115] D. A. Rowlands *et al.*, Phys. Rev. B **72**, 045101 (2005).

[116] D. A. Rowlands, Rep. Prog. Phys. **72**, 086501 (2009).

[117] D. Ködderitzsch, H. Ebert, D. A. Rowlands, and A. Ernst, New Journal of Physics **9**, 81 (2007).

[118] D. A. Biava *et al.*, Phys. Rev. B **72**, 113105 (2005).

[119] D. A. Rowlands, A. Ernst, B. L. Györffy, and J. B. Staunton, Phys. Rev. B **73**, 165122 (2006).

[120] S. Blügel, in *30. Ferienkurs des Instituts für Festkörperforschung 1999 "Magnetische Schichtsysteme"*, edited by Forschungszentrum Jülich GmbH, Institut für Festkörperforschung (Forschungszentrum Jülich GmbH, Jülich, 1999), p. C1.1.

[121] L. Szunyogh, B. Újfalussy, and P. Weinberger, Phys. Rev. B **51**, 9552 (1995).

[122] G. H. O. Daalderop, P. J. Kelly, and M. F. H. Schuurmans, Phys. Rev. B **42**, 7270 (1990).

[123] B. Ujfalussy, L. Szunyogh, and P. Weinberger, Phys. Rev. B **54**, 9883 (1996).

[124] J. B. Staunton *et al.*, Phys. Rev. B **74**, 144411 (2006).

[125] J. B. Staunton *et al.*, Phys. Rev. Letters **93**, 257204 (2004).

[126] S. Bornemann *et al.*, Eur. Phys. J. D **45**, 529 (2007).

[127] K. Sato, P. H. Dederichs, and H. Katayama-Yoshida, Physica B **376-377**, 639 (2006).

[128] M. Toyoda, H. Akai, K. Sato, and H. Katayama-Yoshida, phys. stat. sol. (c) **3**, 4155 (2006).

[129] V. P. Anisimov, B. N. Harmon, and A. N. Smirnov, J. Magn. Magn. Materials **200**, 148 (1999).

[130] M. Pajda *et al.*, Phys. Rev. Letters **85**, 5424 (2000).

[131] E. I. Isaev *et al.*, Phys. Rev. B **65**, 024435 (2001).

[132] F. Maccherozzi *et al.*, Phys. Rev. Letters **101**, 267201 (2009).

[133] B. Lazarovits, L. Szunyogh, and P. Weinberger, Phys. Rev. B **67**, 24415 (2003).

[134] S. Polesya *et al.*, Europhys. Lett. **74**, 74 (2006).

[135] O. Sipr, S. Polesya, J. Minar, and H. Ebert, J. Phys.: Condensed Matter **19**, 446205 (2007).

[136] L. Udvardi, L. Szunyogh, K. Palotas, and P. Weinberger, Phys. Rev. B **68**, 104436 (2003).

[137] H. Ebert and S. Mankovsky, Phys. Rev. B **79**, 45209 (2009).

[138] A. Antal *et al.*, Phys. Rev. B **77**, 174429 (2008).

[139] S. Mankovsky *et al.*, Phys. Rev. B **80**, 014422 (2009).

[140] V. P. Antropov *et al.*, Phys. Rev. B **54**, 1019 (1996).

[141] H. Ebert, Phil. Mag. **88**, 2673 (2008).

[142] M. Matsumoto, J. B. Staunton, and P. Strange, J. Phys.: Condensed Matter **2**, 8365 (1990).

[143] M. Deng, H. Freyer, and H. Ebert, Solid State Commun. **114**, 365 (2000).

[144] M. Deng, H. Freyer, J. Voitländer, and H. Ebert, J. Phys.: Condensed Matter **13**, 8551 (2001).

[145] S. Mankovsky and H. Ebert, Phys. Rev. B **74**, 54414 (2006).

[146] J. Benkowitsch and Winter, J. Phys. F: Met. Phys. **13**, 991 (1983).

[147] E. Stenzel and H. Winter, J. Phys. F: Met. Phys. **15**, 1571 (1985).

[148] W. H. Butler, Phys. Rev. B **31**, 3260 (1985).

[149] P. R. Tulip *et al.*, Phys. Rev. B **77**, 165116 (2008).

[150] X. G. Zhang and W. H. Butler, Phys. Rev. B **51**, 10085 (1995).

[151] W. H. Butler *et al.*, J. Appl. Physics **79**, 5282 (1996).

[152] P. Weinberger *et al.*, J. Phys.: Condensed Matter **8**, 7677 (1996).

[153] T. Huhne and H. Ebert, Phys. Rev. B **60**, 12982 (1999).

[154] L. Szunyogh and P. Weinberger, J. Phys.: Condensed Matter **11**, 10451 (1999).

[155] A. Vernes, L. Szunyogh, and P. Weinberger, J. Phys.: Condensed Matter **13**, 1529 (2001).

[156] A. Vernes, L. Szunyogh, and P. Weinberger, Phys. Rev. B **66**, 214404 (2002).

[157] H. U. Baranger and A. D. Stone, Phys. Rev. B **40**, 8169 (1989).

[158] P. Mavropoulos, N. Papanikolaou, and P. H. Dederichs, Phys. Rev. B **69**, 125104 (2004).

[159] W. H. Butler, J. MacLaren, and X. G. Zhang, Mat. Res. Soc. Symp. Proc. **313**, 59 (1993).

[160] R. H. Brown *et al.*, J. Appl. Physics **81**, 4008 (1997).

[161] P. Zahn *et al.*, Phys. Rev. Letters **80**, 4309 (1998).

[162] H. C. Herper *et al.*, Phys. Rev. B **64**, 184442 (2001).

[163] W. H. Butler, X. G. Zhang, T. C. Schulthess, and J. M. MacLaren, Phys. Rev. B **63**, 054416 (2001).

[164] C. Heiliger, P. Zahn, B. Y. Yavorsky, and I. Mertig, Phys. Rev. B **73**, 214441 (2006).

[165] V. Popescu *et al.*, Phys. Rev. B **72**, 184427 (2005).

[166] R. H. Brown *et al.*, Phys. Rev. B **58**, 11146 (1998).

[167] J. Moser *et al.*, Phys. Rev. Letters **99**, 056601 (2007).

[168] H. Ebert and V. Popescu, International Workshop on Computational Magnetism and Spintronics, MPI Dresden, 2008.

[169] C. Heiliger *et al.*, J. Appl. Physics **103**, 07A709 (2008).

[170] C. Heiliger *et al.*, J. Appl. Physics **103**, 07A709 (2008).

[171] J. J. Rehr, J. Mustre de Leon, S. I. Zabinsky, and R. C. Albers, J. Amer. Chem. Soc. **113**, 5135 (1991).

[172] J. J. Rehr and R. C. Albers, Rev. Mod. Phys. **72**, 621 (2000).

[173] C. R. Natoli, Physica B **208-209**, 5 (1995).

[174] K. Hatada, K. Hayakawa, M. Benfatto, and C. R. Natoli, J. Phys.: Condensed Matter **21**, 104206 (2009).

[175] P. J. Feibelman and D. E. Eastman, Phys. Rev. B **10**, 4932 (1974).

[176] P. J. Durham, J. Phys. F: Met. Phys. **11**, 2475 (1981).

[177] H. Ebert and J. Schwitalla, Phys. Rev. B **55**, 3100 (1997).

[178] J. Henk, A. Ernst, and P. Bruno, Phys. Rev. B **68**, 165416 (2003).

[179] C. R. Ast *et al.*, Phys. Rev. Letters **98**, 186807 (2007).

[180] B. Ginatempo, P. J. Durham, and B. I. Györffy, J. Phys.: Condensed Matter **1**, 6483 (1989).

[181] F. Manghi *et al.*, Phys. Rev. B **59**, 10409 (1999).

[182] J. Braun *et al.*, Phys. Rev. Letters **97**, 227601 (2006).

[183] L. Plucinski *et al.*, Phys. Rev. B **78**, 035108 (2008).

[184] T. Fujikawa and H. Arai, J. Electron. Spectrosc. Relat. Phenom. **174**, 85 (2009).